1521-009X/50/5/519–528$35.00
DRUG METABOLISM AND DISPOSITION
dx.doi.org/10.1124/dmd.121.000789
Drug Metab Dispos 50:519–528, May 2022

Predicting Regional Respiratory Tissue and Systemic Concentrations of Orally Inhaled Drugs through a Novel PBPK Model[S]

Mayur K. Ladumor and Jashvant D. Unadkat

Department of Pharmaceutics, School of Pharmacy, University of Washington, Seattle, Washington

Received November 24, 2021; accepted February 22, 2022

ABSTRACT

Oral inhalation (OI) of drugs is the route of choice to treat respiratory diseases or for recreational drug use (e.g., cannabis). After OI, the drug is deposited in and systemically absorbed from various regions of the respiratory tract. Measuring regional respiratory tissue drug concentrations at the site of action is important for evaluating the efficacy and safety of orally inhaled drugs (OIDs). Because such a measurement is routinely not possible in humans, the only alternative is to predict these concentrations, for example by physiologically based pharmacokinetic (PBPK) modeling. Therefore, we developed an OI-PBPK model to integrate the interplay between regional respiratory drug deposition and systemic absorption to predict regional respiratory tissue and systemic drug concentrations. We validated our OI-PBPK model by comparing the simulated and observed plasma concentration-time profiles of two OIDs, morphine and nicotine. Furthermore, we performed sensitivity analyses to quantitatively demonstrate the impact of key parameters on the extent and pattern of regional respiratory drug deposition, absorption, and the resulting regional respiratory tissue and systemic plasma concentrations. Our OI-PBPK model can be applied to predict regional respiratory tissue and systemic drug concentrations to optimize OID formulations, delivery systems, and dosing regimens. Furthermore, our model could be used to establish the bioequivalence of generic OIDs for which systemic plasma concentrations are not measurable or are not a good surrogate of the respiratory tissue drug concentrations.

SIGNIFICANCE STATEMENT

Our OI-PBPK model is the first comprehensive model to predict regional respiratory deposition, as well as systemic and regional tissue concentrations of OIDs, especially at the drug's site of action, which is difficult to measure in humans. This model will help optimize OID formulations, delivery systems, dosing regimens, and bioequivalence assessment of generic OID. Furthermore, this model can be linked with organs-on-chips, pharmacodynamic and quantitative systems pharmacology models to predict and evaluate the safety and efficacy of OID.

Introduction

Oral inhalation (OI) of drugs is the route of choice to treat respiratory diseases (e.g., bronchodilators) and for recreational drug use (e.g., cannabis and nicotine). The advantages of administering drugs via this route are multifold. This route is noninvasive, consumer friendly, and results in rapid onset of action, local effect, and, therefore, reduced systemic side effects (provided systemic absorption is low) (Gardenhire et al., 2017). The respiratory tract is not a homogeneous tissue, and orally inhaled drugs (OIDs) can be differentially deposited and absorbed from various regions of the respiratory tract (Figs. 1 and 2) to produce local or systemic effect (i.e., after reaching the systemic circulation) or both (Gehr, 1994; ICRP, 1995; Derendorf et al., 2006). Often an OID is targeted to specific regions of the respiratory tract based on the condition being treated (e.g., the trachea for tracheomalacia, bronchi for bronchitis and asthma, bronchioles for bronchiolitis obliterans, and alveoli for infections such as COVID-19, emphysema, and pulmonary fibrosis. Thus, a mechanistic understanding of the regional respiratory drug deposition and absorption is crucial to determine local and systemic drug concentrations and, therefore, pharmacodynamics (PD) (i.e., both efficacy and toxicity) of the drug (Mobley and Hochhaus, 2001). Once understood, this mechanistic knowledge can be applied to optimize OID dosing regimens, drug formulation, delivery systems, and evaluate bioequivalence (BE) of a generic OID (Zhao et al., 2019).

Conventionally, regional respiratory drug concentrations are assessed by imaging, and local lung pharmacokinetic (PK) studies (https://www.ema.europa.eu/en/documents/scientific-guideline/guideline-requirements-clinical-documentation-orally-inhaled-products-oip-including-requirements_en.pdf;

This work was supported by the National Institutes of Health [Grant P01DA032507] (to J.D.U.).

This work was presented as follows: Ladumor MK and Unadkat JD (2021) Predicting regional respiratory tissue and systemic concentrations of orally inhaled drugs through a novel PBPK model. *24th North American ISSX Meeting*; 2021 Sep 13–17. International Society for the Study of Xenobiotics, Washington, D.C.

dx.doi.org/10.1124/dmd.121.000789.

[S] This article has supplemental material available at dmd.aspetjournals.org.

ABBREVIATIONS: AL, alveolar or pulmonary; AUC, area under the curve; BB, bronchial; bb, bronchiolar; BDP, beclomethasone dipropionate; BE, bioequivalence; 17-BMP, beclomethasone 17-monopropionate; DF, deposition fraction; DF_{scalar}, deposition fraction scalar; DMET, drug-metabolizing enzymes and transporters; ELF, epithelial lining fluid; ET1, extrathoracic (nasal passage); ET2, extrathoracic (oral passage); fa_{gut}, fraction drug absorbed from the gut; f_{hyg}, hygroscopic growth factor; ICRP, international commission on radiological protection; IVIVE, in vitro to in vivo extrapolation; MMAD, mass median aerodynamic diameter; OCT, organic cation transporter; OI, oral inhalation; OID, orally inhaled drug; PBPK, physiologically based pharmacokinetic; PD, pharmacodynamics; PK, pharmacokinetic; P_{scalar}, permeability scalar; RB, relative to the baseline.

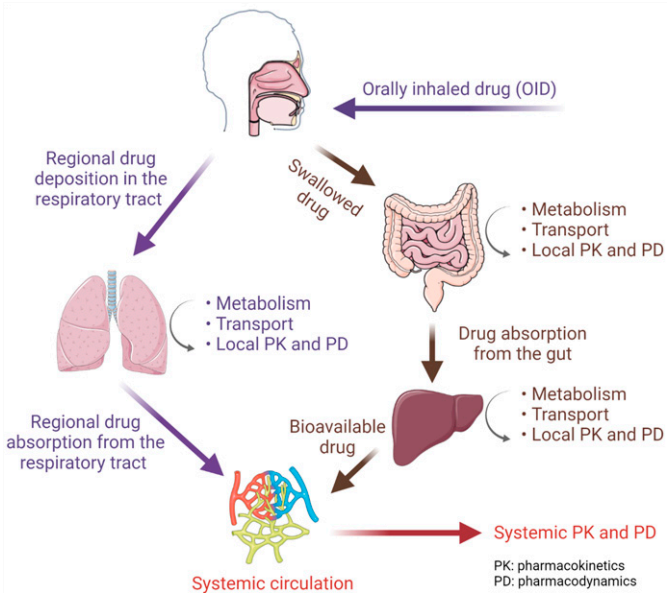

Fig. 1. Drug movement pathway from the oral inhalation device to the respiratory tract and eventually to the systemic circulation.

Sadiq et al., 2021). Such studies are costly, and therefore not possible to implement routinely. In addition, local PK studies are invasive, and the measured concentration-time data are usually sparse. Another approach is to scale local PK in animals to humans. However, when enzymes and transporters are involved, such allometric scaling may not be accurate. Unlike the above studies, systemic PK studies do not provide a measure of the regional respiratory drug concentrations (https://www.ema.europa.eu/en/documents/scientific-guideline/guideline-requirements-clinical-documentation-orally-inhaled-products-oip-including-requirements_en.pdf) and, therefore, cannot be used as a surrogate measure of the PD of the drug in the respiratory tissue. Even when the target site of the OID is systemic (i.e., not in the respiratory tract), plasma drug concentrations are not always measurable after OI of the drug. In that event, this classic systemic PK approach cannot be used to assess bioavailability of the OID or BE assessment of a generic version of the OID. Even if the systemic PK of the OID are measurable, they may not be a surrogate of the respiratory target site drug concentrations and, therefore, the PD of the drug (Hendrickx et al., 2018; Newman and Witzmann, 2020). In such cases, to demonstrate BE of a generic OID, PD effect or comparative clinical endpoint can be used as a surrogate of local respiratory drug concentrations. However, unless the PD effect or clinical comparative endpoint is readily quantifiable, this approach is not feasible and, even if feasible, potentially costly (Newman and Witzmann, 2020).

To overcome some of the above deficiencies of routine PK studies of OID, a promising alternative approach is to predict local and systemic drug concentrations and, therefore, the PD of an OID through physiologically based pharmacokinetic (PBPK) modeling and simulation (Zhao et al., 2019). However, for such a model to have reliable predictive success, it must incorporate fundamental processes that affect the respiratory drug deposition, absorption, and local as well as systemic drug concentrations (Boger et al., 2016; Haghnegahdar et al., 2019; Hartung and Borghardt, 2020; Yu and Rosania, 2010; Gaohua et al., 2015; al.; Eriksson et al., 2020; Melillo et al., 2020; Miller et al., 2022; Shao et al., 2021). Several commercial and open-source OI-PBPK models are available (Bäckman et al., 2018; Borghardt et al., 2015). However, these models have several limitations, namely: (1) incomplete inclusion of important regions of the respiratory tract; (2) lack of hygroscopic particle growth to predict respiratory deposition of a highly water-soluble drugs (e.g., nicotine); (3) lack of monitoring of hydrolyzed or metabolized product(s) (active or toxic) in epithelial lining fluid (ELF) of the respiratory tract, a feature especially important when the OID is a prodrug and the active moiety is the hydrolyzed product [e.g., beclomethasone dipropionate (BDP) and its active moiety such as beclomethasone 17-monopropionate (17-BMP)]; and (4) lack of incorporation of tissue retention to accurately predict local concentration and absorption of the drug (e.g., budesonide). Therefore, the goals of the present study were to (1) develop a regional OI-PBPK model, which incorporates all the above-listed features, to predict regional respiratory drug deposition and local and systemic concentrations of an OID; (2) validate these predictions using the two OIDs, morphine and nicotine; and (3) conduct a sensitivity analysis to determine which drug and physiologic parameters are important for regional and systemic drug exposure and therefore PD of an OID.

Materials and Methods

OI Model Structure and Assumptions. Our OI model consists of four regions (Figs. 2 and 3) based on the human respiratory tract model of the International Commission on Radiologic Protection publication 66 (ICRP 66) (ICRP, 1995). It includes the extrathoracic (ET) and thoracic airways. The ET airway includes the nasal passages (ET1, anterior nose) and oral passages (ET2, includes the posterior nasal passages, larynx, pharynx, and mouth). The thoracic airway (also commonly known as lung) includes the bronchial [BB, which consists of the trachea (airway generation 0) and the bronchi (airway generations 1–8)]; the bronchiolar [bb, consisting of the bronchioles and terminal bronchioles (airway generations 9–15)]; and the alveolar [AL, includes the respiratory bronchioles, alveolar ducts, and sacs with their alveoli (airway generations 16 and beyond)] regions (Fig. 2A). The term "airway generation" refers to the point at which an airway separates into two or smaller airways. The BB and bb regions are collectively referred as the tracheobronchial or central region, whereas the AL region is known as the pulmonary or peripheral region. The ET1 region was ignored in the current OI model because it is important for drug administration through nasal inhalation but not for OI. However, if necessary, it can be integrated into the current PBPK model. This OI model was created using MATLAB (version R2021) and its SimBiology module (Mathworks, MA). The rate equations were solved using the ode15s solver. Detailed information on model equations and systems parameters of the ICRP reference adult male are provided in the Supplemental Material (Supplemental Method and Supplemental Tables 1–5). As described below, each region was further subdivided into five compartments (i.e., airway lumen, ELF, epithelial, subepithelial, and blood) (Fig. 3).

Airway Lumen Compartment. The regional dose exposure for each respiratory tract region was calculated by multiplying the regional deposition fraction (DF, percentage of the total amount of inhaled drug that is deposited in various regions of the respiratory tract) with the overall OI dose. In the absence of in vivo regional DF data obtained through imaging studies, deposition of drug in the airway lumen of the human respiratory tract was calculated using the in silico ICRP 66 deposition model (ICRP, 1995). Briefly, the ICRP 66 deposition model calculates the DF for each respiratory tract region (ET2, BB, bb, and AL) using algebraic equations built from experimental and theoretical data (Supplemental Method and Supplemental Tables 1–3). The ICRP 66 deposition model considers breathing maneuvers (mentioned below) based on various activities such as sleep, sitting or resting, light exercise, and heavy exercise for nasal and mouth breathers. Here, we used the ICRP 66 deposition model to predict regional deposition of OID for a mouth breather who is seated. The ICRP 66 deposition model is applicable to particles with diameters ranging from 0.001 to 100 μm (ICRP, 1995). To determine the extent and pattern of drug deposition of OID (solid or liquid) from an OI delivery device, the ICRP 66 deposition model requires the following information: (1) aerodynamic particle size distribution parameters including mass median aerodynamic diameter (MMAD, the diameter at which 50% of the particles/droplets in an aerosol are larger and 50% are smaller) and geometric standard deviation of the aerodynamic diameter (measures the dispersion of particle/droplet diameter); (2) drug particle/droplet density; (3) drug particle/droplet shape; (4) volumetric or inhalation flow (the volume of air that travels

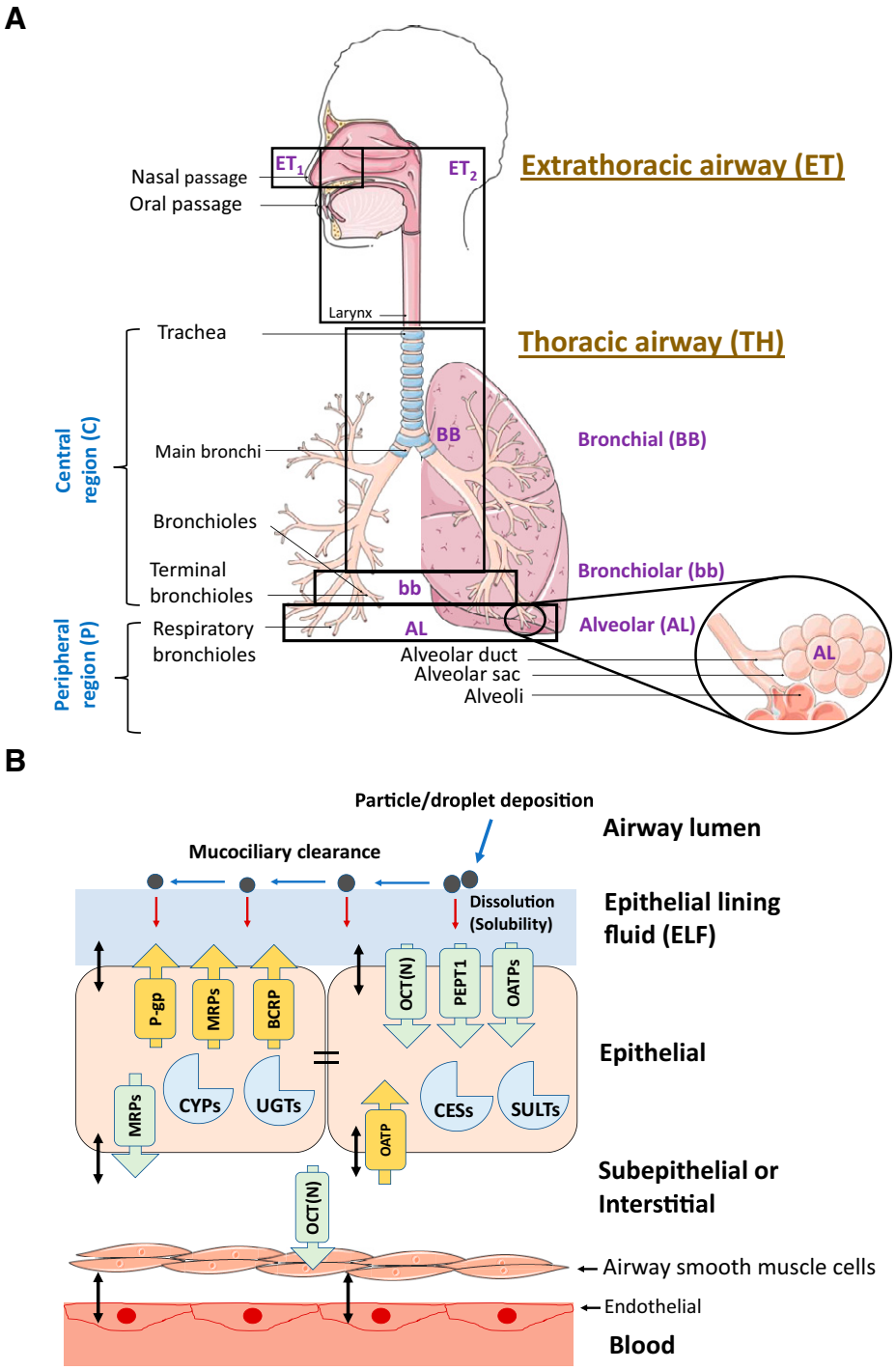

Fig. 2. Regional classification of the human respiratory tract (A) and the processes that determine the movement of drugs through different layers of each region (B). Transporter and enzymes listed in (B) are examples and not a comprehensive list. C, central region (BB+bb); P, peripheral region (AL); P-gp, P-glycoprotein; MRP, multidrug resistance-associated protein; BCRP, breast cancer resistance protein; OCT, organic cation transporter; OCTN, organic cation/carnitine transporter; PEPT1, peptide transporter 1; OATP, organic-anion-transporting polypeptides; C Y P , cytochrome P450; UGT, UDP-glucuronosyltransferase; CES, carboxylesterases; SULT, sulfotransferase.

per unit of time); (5) physiologic parameters such as tidal or inhalation volume (the volume of air that enters or exits the lungs during each respiratory cycle), functional residual capacity (volume of air remaining in the lungs after passive expiration), and dead space volume (the volume of air inhaled that does not participate in gas exchange); (6) anatomy parameter such average diameter of the different regions of the respiratory tract; and (7) hygroscopic growth factor (f_{hyg}) information, which is critical for highly water-soluble OI drugs because it can be used to predict diameter changes caused by respiratory tract humidity. The above-mentioned input parameters were collected from literature and ICRP publications 66 and 135 (ICRP, 1995; Paquet et al., 2015) (Supplemental Material 1).

ELF or Airway Liquid Compartment. After drug deposition, the solid drug first dissolves in the ELF [described by the Hintz-Johnson model (Hintz and Johnson, 1989)], where it may be chemically degraded or metabolized (e.g., via hydrolysis). Because the OID may be a prodrug and the metabolite/degradant may be active/toxic, our model included monitoring the concentration of the metabolite/degradant in the ELF. The mucus and aqueous layers were combined into a single ELF and considered to be in instantaneous equilibrium with each other, but dynamic changes in the volume of ELF was not considered because of the lack of information on fluid absorption and secretion. The undissolved or dissolved amount of drug from each compartment travels to the preceding compartment through first-order respiratory transit rate constant [direction: AL to bb (through macrophage clearance), bb to BB (through mucociliary clearance), BB to ET2 (through mucociliary clearance), and ET2 to the gut region (through swallowing)] (ICRP, 1995; Borghardt et al., 2015). The respiratory transit rate

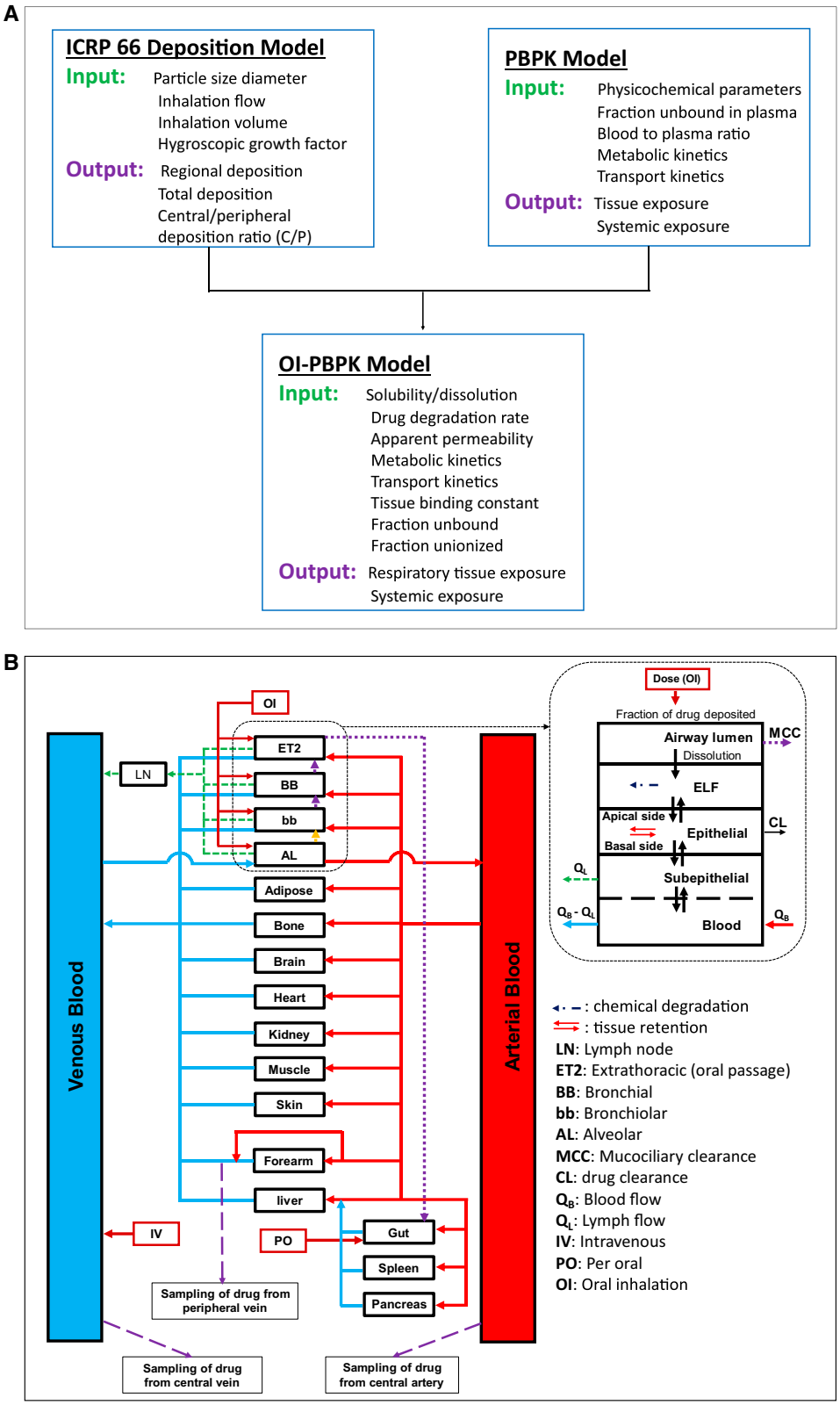

Fig. 3. (A) Schematic workflow for the development of OI-PBPK model with input and output information for the ICRP 66 deposition and PBPK model and (B) the framework for our regional OI-PBPK model. Drug concentration in the peripheral vein (rather than the central vein) and the central artery were sampled.

constants were obtained from the ICRP clearance model (Paquet et al., 2015). The model also included the amount of drug removed from the ET2 region via coughing and exhaled.

Epithelial or Intracellular Compartment. The OID can be actively transported (unbound) or passively transferred (unionized and unbound) in a bidirectional manner across any of the cell membranes (Fig. 2B). Passive apparent permeability was assumed to be bidirectionally the same and scaled based on regional surface area (Gaohua et al., 2015; Melillo et al., 2020). In the epithelial compartment the unbound drug can be metabolized by the enzymes present there (Fig. 2B). The model includes drug tissue retention (e.g., reversible fatty acid conjugation) in localized epithelial tissue of the respiratory system through second-order association and first-order dissociation rate constants (Fig. 2B).

Subepithelial or Interstitial Compartment. The OID can be actively transported (unbound) or bidirectionally passively transferred (unionized and unbound) to the subepithelial compartment through the basal cell membrane. The lymphatic circulation can carry the drug from the subepithelial to the lymph nodes and then to the venous blood.

Blood or Vascular Compartment. Rapid bidirectional transfer between subepithelial and the blood compartment of the drug can be by both para- and transcellular route due to the presence of fenestrated endothelial cells (Kuepfer et al., 2016). Then, the drug can be carried into the arterial and venous blood through the systemic (ET2 region), bronchial (BB and bb regions), and pulmonary (AL region) circulations. The pulmonary circulation carries drugs from the venous blood to the AL regions. In contrast, the bronchial circulation carries drugs from the arterial blood to the BB and bb regions (Baile, 1996). Likewise, systemic circulation carries drugs from the arterial blood to the ET2 region.

Integration of OI Model into a Whole-Body PBPK Model. The OI model was integrated into our previously published PBPK framework (Ke et al., 2012; Ke et al., 2013; Ke et al., 2014; Zhang et al., 2017; Zhang and Unadkat, 2017). The whole-body PBPK model included all the major tissues responsible for drug disposition (Fig. 3). Except for the liver and respiratory tract, drug distribution from the blood into tissues was assumed to be perfusion limited. In the liver, segregated into three sub-compartments (intracellular, interstitial, and vascular), permeability-limitation was allowed. Likewise, in the respiratory tract compartments, permeability limited entry and exit of the drug across the cellular and capillary/endothelial membranes was allowed and was parameterized with respect to Michaelis-Menten parameters (maximum rate of active transport, J_{max}; and Michaelis constant, K_m) or intrinsic clearance (CL_{int}). To describe the absorption of the drug in the gut that was swallowed from the ET2 region, the first-order oral absorption model was implemented. The peripheral arm vein sampling model developed by Huang and Isoherranen was incorporated into the OI-PBPK model (Huang and Isoherranen, 2020).

Development of OI-PBPK Model for Morphine and Nicotine. To develop OI-PBPK model for these drugs, the reported morphine (Emoto et al., 2017) and nicotine (Kovar et al., 2020) PBPK models following their intravenous (IV) administration (see Supplemental Tables 6 and 7 for drug-dependent parameters) were adopted. Then, validation of the OI-PBPK model for morphine and nicotine was conducted as follows.

Estimation of Parameters for the Morphine and Nicotine OI-PBPK Models. (1) regional morphine and nicotine deposition in the respiratory tract following its OI administration via a nebulizer and cigarette, respectively, were predicted using the ICRP 66 deposition model (Supplemental Tables 8 and 9); (2) the in vitro apparent permeability between ELF and epithelial regional for both drugs was predicted using logarithm of octanol-water distribution coefficient at pH 7.4 value through in silico regression model developed using octanol-water distribution coefficient at pH 7.4 and in vitro Calu-3 permeability data (Brillault et al., 2010) (Supplemental Method); (3) regional apparent permeability was calculated by scaling the in vitro apparent permeability of the drug through the epithelial cell thickness of each region of the respiratory tract (Supplemental Method); (4) the in vivo regional permeability of the drug was calculated by the product of the regional apparent permeability and surface area of each region of the respiratory tract (Supplemental Method); (5) the Henderson-Hasselbalch equation (Po and Senozan, 2001) was used to compute the fraction unionization of the drug in each sub-compartment of the OI model using the drug's pKa value (Supplemental Table 10); (6) the fraction unbound of the drug in each subcompartment of the OI model was calculated using the fraction unbound in plasma and the partition coefficient (Supplemental Table 10); (7) the puff frequency and time interval between each puff of the administered OI drug were obtained from the literature (Supplemental Table 13); (8) in vitro to in vivo extrapolation (IVIVE) of the metabolic and/or transporter kinetics of the drug in the respiratory tract was performed using the relative total molar abundance of drug-metabolizing enzymes and transporters (DMET) protein in the various regions of the respiratory tract relative to that in the liver tissue. To do so, we assumed that the catalytic rate constant (k_{cat}) is invariant across all tissues (Supplemental Method). The total molar abundance of DMET protein per tissue (in μmol/tissue unit) was determined by multiplying the abundance of DMET protein in the subcellular fraction (in pmol/mg unit) by the yield of the subcellular fraction per gram of the tissue (in mg/g unit) and the tissue weight (in g unit).

Assumptions for Morphine and Nicotine OI-PBPK Models. For both drugs, the following assumptions were made (1) due to lack of information, chemical degradation/hydrolysis in the ELF compartment and tissue retention of drugs in the epithelial compartment was assumed to be negligible; (2) regional passive permeability between epithelial and subepithelial and subepithelial and blood compartments was assumed to be high (100 cm/s) and not rate limiting; (3) the amount of drug eliminated through coughing was negligible; (4) due to lack of region-specific tissue composition of lipids, proteins, and pH, the fraction unbound and the fraction unionized in each compartment were assumed to be identical for each region of the respiratory tract.

Validation of Morphine and Nicotine OI-PBPK Models. For validation of our OI-PBPK model, the PK endpoints maximum [C_{max} and area under the concentration time curve up to the last measurable concentration (AUC_{last})] of the drugs after their IV and OI administration were simulated and compared with their corresponding observed in vivo values. Our model was considered validated if the ratio of the simulated and the observed PK endpoints fell within 0.8–1.25 (Ladumor et al., 2019a; Ladumor et al., 2019b).

Sensitivity Analysis to Assess the Impact of Drug and Physiologic Parameters on Respiratory Drug Deposition and Systemic Absorption. A sensitivity analysis was performed to demonstrate the impact of drug and physiologic parameters on the regional deposition, regional tissue concentration, and systemic absorption after OI of hypothetical drugs X and Y (modeled based on morphine, i.e., input to the OI-PBPK model were assumed to be identical to morphine except as noted below). The following additional assumptions are made for the hypothetical drugs X and Y: (1) Drug X was administered as a solid form through an inhaler, and its regional absorption was assumed to be a limited by its solubility in the ELF; (2) drug Y was assumed to be permeability-limited, metabolized in the respiratory tissues, binds with fatty acid in the epithelial region of the respiratory tract, and administered as a solution through a nebulizer. The deterministic parameters of both these formulations were MMAD, inhalation flow, inhalation volume, f_{hyg}, drug dissolution, tissue retention, and DMET kinetics, based on literature (Brand et al., 2005; Derendorf et al., 2006; Zhang et al., 2006; Borghardt et al., 2015; Ehrhardt et al., 2017). Therefore, these parameters were included in our sensitivity analysis and their values varied between two and five times of the value used for morphine. Then, they were integrated into the OI-PBPK model to predict the drug's respiratory deposition, local tissue and systemic exposure.

Results

Comparison of the OI-PBPK Model-Predicted and Observed Plasma Concentration of Morphine or Nicotine after IV Administration. Using our OI-PBPK model, we reproduced the predicted mean plasma concentration-time data published by others following IV administration of morphine (Fig. 4A) or nicotine (Fig. 5A). The predicted-to-observed values (C_{max} and AUC_{last}) fell within our a priori acceptance criterion (0.8–1.25) (Supplemental Tables 11 and 12).

Prediction of Systemic Exposure to Nebulized Morphine after OI. The OI-PBPK model predicted that 53% of the nebulized morphine was deposited in the respiratory tract while the remainder (47%) was exhaled (Supplemental Table 8). This deposition followed the order ET2 (19.2%) > AL (10.4%) > BB (16.0%) > bb (7.1%) (Supplemental Table 8). When f_{hyg} was not included in the model, the simulated PK endpoints (C_{max} and AUC_{last}) of morphine after OI were underpredicted as compared with observed data (Dershwitz et al., 2000) (Supplemental Table 11). After including f_{hyg} (=3) (Supplemental Table 8), the change in the predicted percent total and regional deposition increased [total: 72.9%; ET2 (33.0%) > AL (12.3%) > BB (19.5%) > bb (8.1%)]. However, the predicted PK endpoints remained underestimated (Supplemental Table 11). After integrating a permeability scalar (P_{scalar}, 5) to the in vitro apparent permeability of morphine between ELF and epithelial regional compartments, the predicted PK endpoints fell within 0.8- to 1.25-fold of the observed values (Supplemental Table 11).

Prediction of Systemic Exposure to Nicotine after Cigarette Smoking. The OI-PBPK model predicted a total of 55.7% of nicotine was deposited in the respiratory tract and the remaining 44.3% exhaled (Supplemental Table 9). The predicted regional deposition of nicotine

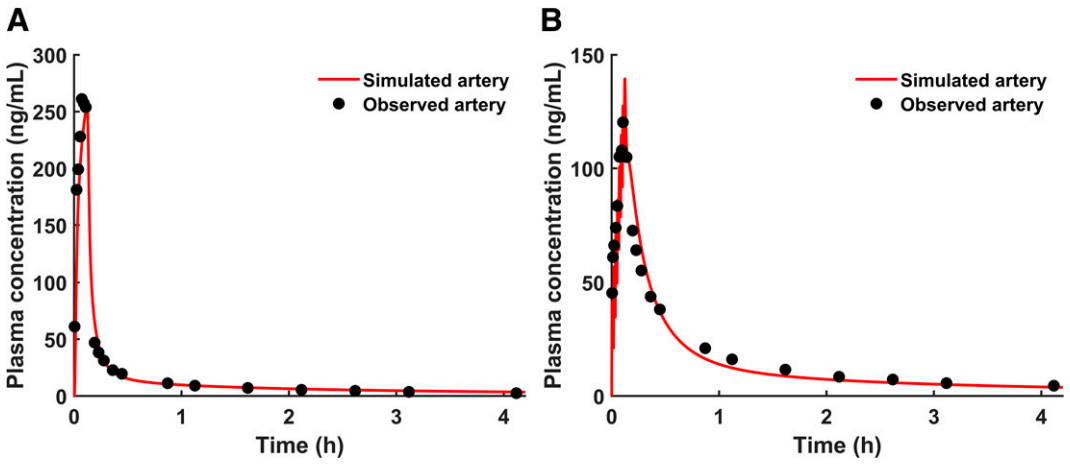

Fig. 4. Representative OI-PBPK model simulated and observed arterial morphine plasma concentrations after (A) intravenous (8.8 mg over 0.16 hour) or (B) oral inhalational (17.6 mg, 8 inhalation doses with 1-minute interval) administration (nebulizer). Drug concentration in the central artery was sampled. The predicted-to-observed values (C_{max} and AUC) fell within our a priori acceptance criterion (0.8–1.25) (Supplemental Table 11).

in the respiratory tract followed the order bb (31.3%) > AL (21.4%) > BB (2.0%) > ET2 (1.0%). Using these data, the systemic exposure of nicotine following OI administration was underpredicted. After including the reported f_{hyg} (= 1.7) (Schroeter et al., 2001) of nicotine in the model (Supplemental Table 9), the change in the predicted percent total and regional deposition improved [total: 64%; bb (41.1%) > AL (20.8%) > BB (1.3%) > ET2 (0.7%)] when compared with the measured in vivo values (Supplemental Table 9) but the systemic exposure remained underestimated. However, after including an empirical DF scaling factor (DF_{scalar}, 1.5), the predicted total and regional deposition fractions were in good agreement with those measured in vivo (Supplemental Table 9). With this scaling, the final predicted total and regional depositions of smoked nicotine were 96% and followed the order bb (61.7%) > AL (31.2%) > BB (2.0%) > ET2 (1.1%) (Supplemental Table 9). Then, the simulated nicotine plasma concentration-time profiles after OI administration (cigarette smoking) fell within 1.25-fold of the observed values (Fig. 5 and Supplemental Table 13).

Sensitivity Analyses of the Impact of Drug and Physiologic Parameters on Respiratory Deposition and Systemic Absorption of OID. With an increase in MMAD, hypothetical drug X deposition increased in the ET2 and BB region but decreased in the AL region. Also, the ratio of deposition in the central to peripheral region (C:P ratio) increased with an increase in MMAD (Fig. 6A). As a result, due to the rapid dissolution in the airway fluid, the C_{max} and AUC_{last} of drug X were decreased and increased, respectively (Fig. 6b). In contrast, no change in the PK endpoints was observed when fraction of oral gut absorption (fa_{gut}) was set to zero (Fig. 6b). However, when poor dissolution was assumed, all the PK endpoints of drug X increased (Fig. 6c). The PK endpoints returned to baseline when oral gut absorption was set to zero (Fig. 6c). Also, with a decrease in MMAD, the overall and regional deposition decreased but the relative AL deposition increased compared with other respiratory regions such as ET2. Hence, the C:P ratio decreased (Fig. 6a). This led to a decline in PK endpoints but no change in PK endpoints when dissolution rate and mucociliary clearance were altered.

A decrease in the inhalation flow resulted in a higher fraction of drug X deposited in the ET2 and BB regions and higher C:P ratio (>1). Due to this, C_{max} decreased but AUC_{last} modestly increased (Supplemental Fig. 1A). An increase in the inhalation flow resulted in a higher fraction of drug X deposited in the AL region [relative to the baseline (RB), approximately twofold] and lower C:P ratio (<1). Consequently, C_{max} increased (RB, ∼1.5-fold), but AUC_{last} did not change (Supplemental Fig. 1A).

As inhalation volume was increased, deposition of drug X in the AL region increased (RB, approximately twofold) resulting in a lower C:P ratio and higher C_{max} (RB: ∼1.5-fold) but no change in AUC_{last} (Supplemental Fig. 1B). When the inhalation volume was decreased, deposition of drug X in the AL region decreased, but drug deposition in remaining regions did not change or slightly increased, resulting in a higher C:P ratio, and C_{max} decreased, but AUC_{last} modestly increased (Supplemental Fig. 1B).

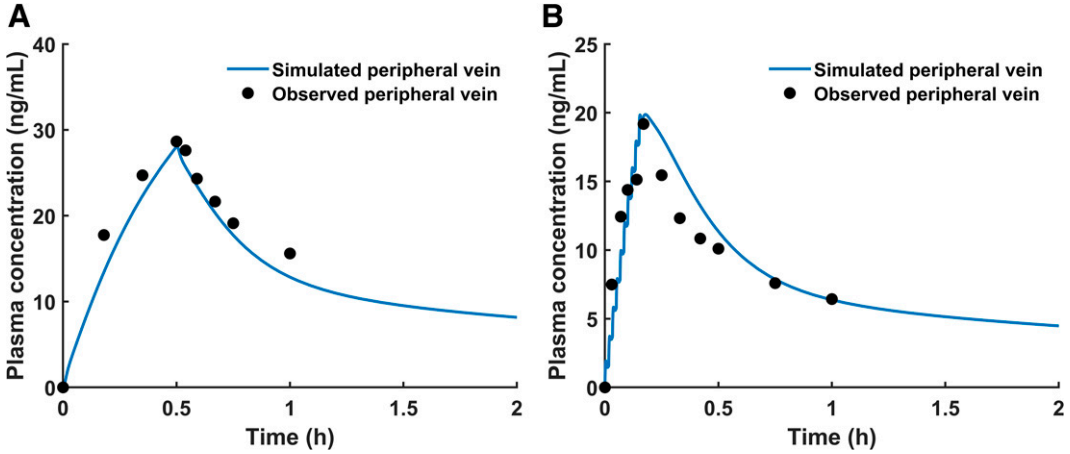

Fig. 5. Representative OI-PBPK model simulated and observed peripheral venous nicotine plasma concentrations after (A) intravenous (4.38 mg over 0.5 hour) or (B) oral inhalational (2.2 mg, multiple dosing) administration (cigarette smoking). Drug concentration in the peripheral vein (rather than the central vein) was sampled. The predicted-to-observed values (C_{max} and AUC_{last}) fell within our a priori acceptance criterion (0.8–1.25). Although our model was validated using data from a number of intravenous and oral inhalational studies (Supplemental Tables 12 and 13), only the observed data from Gourlay et al. (1997) are shown.

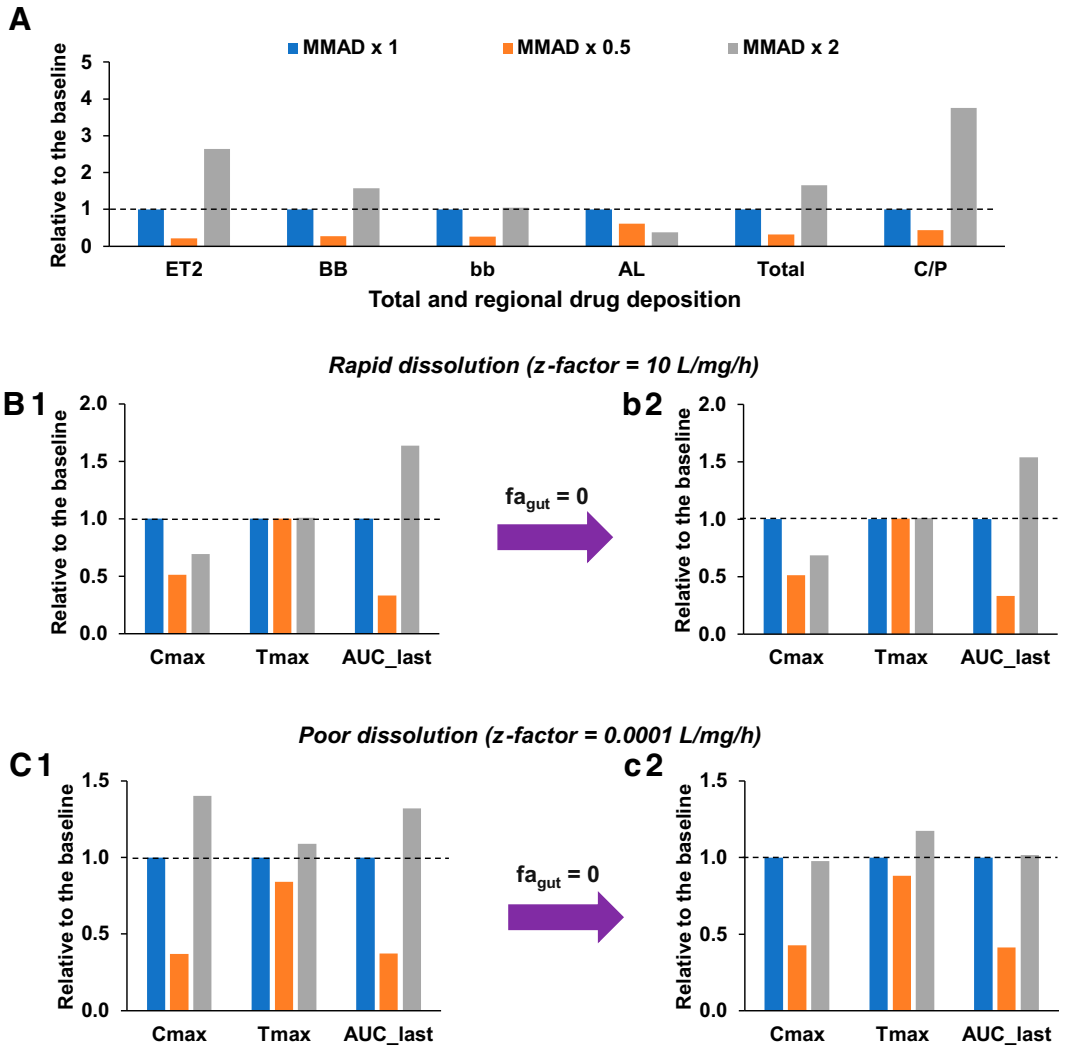

Fig. 6. Sensitivity analyses to demonstrate the impact of change in MMAD on (A) total and regional respiratory tract deposition, and pharmacokinetics (PK) endpoints of drug X with (B1 and B2) rapid dissolution in the airway fluid (z-factor = 10 L/mg/h) without and with no oral gut absorption (fa_{gut} = 0), and (C1 and C2) poor dissolution in the airway fluid (z-factor = 0.0001 L/mg/h) without and with no oral gut absorption (fa_{gut} = 0). z-factor, dissolution rate constant.

An increase in the hygroscopic growth factor resulted in a higher total and regional deposition in the ET2 region and resulted in higher AUC_{last} but a minor change in C_{max} (Supplemental Fig. 1C).

Increased apical influx and efflux transporter activity at epithelial and subepithelial membranes resulted in increased and decreased systemic and regional exposure of drug Y, respectively, (Supplemental Figs. 2 and 3). Likewise, increased metabolism resulted in a decrease in both systemic and regional tissue exposure of drug Y (Supplemental Fig. 4). The increased dissociation rate constant in the epithelial region resulted in an increased systemic and regional C_{max} but no change in exposure of drug Y (Supplemental Fig. 5).

A decrease in the dissolution rate (z-factor) of drug X (solid formulation as opposed to the liquid nebulizer formulation of drug X) resulted in a decrease in both C_{max} and AUC_{last} (Supplemental Fig. 6).

Discussion

In the present study, we developed an OI-PBPK model to predict drug deposition and absorption and the resulting respiratory tissue and systemic drug concentrations of OIDs. Our model was developed using the ICRP 66 deposition and clearance model (ICRP, 1995; Paquet et al., 2015). The in vitro data required by our OI-PBPK model are aerodynamic particle size distribution parameters, inhalation flow, inhalation volume, dissolution (solubility), permeability, fraction unbound/unionized, and metabolic and transport kinetics. All these values are available, whether from the literature, estimated using in silico methods, or determined from in vitro studies of the drug.

Our OI-PBPK model can be distinguished from the existing OI-PBPK models by several features. First, our model accounts for the hygroscopic growth of particles to predict regional deposition of water-soluble hygroscopic drugs (ICRP, 1995; Chalvatzaki and Lazaridis, 2018). Second, our model can monitor drug degradation kinetics in the ELF. For example, BDP is hydrolyzed to its metabolite, 17-BMP, in the intestinal fluid, which also indicates possible degradation in ELF, which has a comparable pH of 6.5 (Würthwein and Rohdewald, 1990). Third, our model accounts for tissue retention relevant to inhaled corticosteroids (e.g., budesonide) that can reversibly conjugate with fatty acid esters present in the epithelial region. This conjugation will prolong the mean residence time of the drug in the lung tissue (Miller-Larsson et al., 1998) (Supplemental Fig. 5). Fourth, our model includes solubility and dissolution processes important for orally inhaled suspension or dry powder formulation. For example, inhaled corticosteroids (e.g., BDP) are highly lipophilic (Kumar et al., 2017), where dissolution/solubility is the rate-limiting steps in their absorption (Supplemental Fig. 6). Hence, dissolution (solubility) processes are important to include in OI-PBPK models to reliably predict tissue and systemic concentrations of these drugs.

Fifth, the volume of each compartment was estimated based on compartment thickness, which is critical for prediction of regional respiratory tissue drug concentrations. Last, but not least, our model accounts for regional transport and metabolic processes, crucial to determine local tissue concentrations of OID (Supplemental Figs. 2–5). For example, drugs can be actively transported through apical P-glycoprotein efflux transporter (e.g., BDP, ciclesonide, and budesonide) and/or apical organic cation transporter (OCT) influx transporter (e.g., albuterol, formoterol, ipratropium, and tiotropium bromide) present in the epithelia of the respiratory tract tissues (Bosquillon, 2010; Crowe and Tan, 2012; Ehrhardt et al., 2017). Also, our model allows incorporation of transporters in the subepithelial compartment (e.g., airway smooth muscle cells), a site of action for many OIDs (Supplemental Fig. 3). For example, organic cation/carnitine transporters, present in the subepithelial regions (e.g., airway smooth muscle cells), are a target for inhaled bronchodilator drugs (e.g., albuterol) (Horvath et al., 2007). Moreover, a few OIDs are metabolized in the epithelia of the lung by phase I and phase II DME, such as esterase that hydrolyze prodrugs to their pharmacologically active metabolites (e.g., prodrug BDP and its metabolite 17-BMP) (Somers et al., 2007; Olsson et al., 2011; Oesch et al., 2019).

For validation of our OI-PBPK model, we used the PK bioequivalence criterion (i.e., predicted systemic exposure within 0.85- to 1.25-fold of the observed value) to assess the success of the simulation. Our OI-PBPK model was validated using systemic mean morphine and nicotine exposure rather than respiratory tissue exposure, because the latter is not available. Our prediction for systemic exposure to morphine following OI administration via nebulizer was improved after integrating f_{hyg} and P_{scalar} in our model. The need to incoprorate f_{hyg} is not surprising, because morphine is a water-soluble drug (64 mg/ml water solubility), and the nebulized solution is mixed with saline (sodium chloride, NaCl) (Schuster et al., 1997; Dershwitz et al., 2000). NaCl is hygroscopic and exhibits a two- to fourfold higher in particle diameter upon inhalation (ICRP, 1995). As a result, it may have an effect on the amount of drug deposited in the respiratory tract, as shown in the literature for commercial nebulizer formulations (Haddrell et al., 2014). In addition, morphine is a substrate of OCT1 and UGT2B7 (Emoto et al., 2018), expressed in the respiratory tract (Sakamoto et al., 2013). The systemic PK parameters of morphine were underpredicted after integrating morphine DMET kinetics in our OI model. Therefore, to recover the observed systemic morphine PK profile, we needed to apply a P_{scalar} value to the in vitro apparent permeability at apical epithelial membrane perhaps because our IVIVE of morphine transport kinetics was not accurate. For nicotine, besides including $f_{hyg,}$ the deposition fraction needed to be scaled by DF_{scalar} to recover the in vivo deposition of the drug. This may be due to the fact that ICRP 66 deposition model does not take into account cloud dynamics of smoked aerosol and the DF_{scalar} indirectly represents these mechanisms in the model. Interestingly, we found that the impact of lung metabolism and/or transport on systemic PK of nicotine and morphine was minimal (data not shown), likely due to the low expression of DMET proteins in lungs.

In our sensitivity analysis, we showed the impact of drug and physiologic parameters on drug deposition as well as respiratory and systemic drug concentrations. Some studied parameters, e.g., MMAD, inhalation flow, and inhalation volume, affected drug deposition and therefore the PK endpoints. For example, increased MMAD resulted in greater deposition of drug X in total, including the ET2 and BB regions, but lower deposition in the AL region (Fig. 6A), most likely due to increased particle impaction caused by the increased particle size (Brand et al., 2005). This resulted in an increased AUC_{last} of drug X driven by greater total deposition and a lower C_{max} driven by lower deposition in the AL region (Fig. 6B). No change in the PK endpoints was observed when fa_{gut} was set to zero. This suggests that all the drug is dissolved in the airway fluid and there is little drug cleared by mucociliary clearance to the GI tract (Fig. 6B). However, when we assumed poor drug dissolution rate in the airway fluid then the PK endpoints were increased with increase in MMAD, likely because mucociliary clearance transferred undissolved drug to the GI tract (Fig. 6C). Indeed, the PK endpoints did not increase with increase in MMAD when oral gut absorption was set to zero (Fig. 6C). This again highlights the role of mucocilliary clearance in interpreting PK data of OI drugs. With reduced MMAD, the total deposition decreased, but AL deposition increased relative to other regions (e.g., ET2) likely due to increased particle sedimentation in the AL region driven by the smaller particle size. This resulted in decreased PK endpoints as driven by lower total deposition but little or no change in PK endpoints with different dissolution conditions and mucociliary clearance because these parameters mostly affect drug absorbed from the ET2 region which was minimal due to reduced deposition in this region (Fig. 6).

Similar trends were obtained with inhalation flow rate. Reduced flow rate resulted in greater deposition in the AL region and therefore greater C_{max} due to rapid absorption of the drug from the AL region, which has a greater surface area. AUC_{last} did not change likely because the drug's total deposition was similar to that obtained with the other flows (Supplemental Fig. 1A). Similarly, increased inhalation volume, resulted in higher deposition in AL region, likely due to particle sedimentation. As a result, C_{max} was increased (due to larger AL surface area and higher drug AL deposition), leading to higher rate and somewhat higher extent (AUC) of drug absorption (Supplemental Fig. 1B). Increased hygroscopic growth resulted in increased particle size due to impaction, and therefore higher total drug deposition in the ET2 region as well as total. As a result, AUC_{last} increased as driven by total deposition (Supplemental Fig. 1C). A modest increase in C_{max} is likely due to slightly increased drug deposition in AL region and therefore increased rate of absorption from this region (higher surface area). The latter was not observed with an increase in MMAD because that was accompanied by a reduction in AL drug deposition (Fig. 6A).

We also explored the impact of metabolism and transport on respiratory tissue and systemic drug concentrations. Variability in DMET protein abundance in the respiratory tract can alter the drug concentration at target site and therefore drug response. We found that increased influx or efflux apical epithelial or subepithelial membrane transporter activity resulted in either increased (influx) or reduced (efflux) drug Y epithelial or subepithelial concentrations in all the regions of the respiratory tract (Supplemental Figs. 2 and 3). We found that increased drug metabolic activity in the epithelial region, decreased systemic and regional exposure of drug Y (Supplemental Fig. 4). In contrast, as expected, increased dissociation rate of the drug from its intracellular binding to fatty acids, resulted in an increase in systemic and regional C_{max} but no change in local or systemic exposure as measured by AUC_{last} (Supplemental Fig. 5). Also, we found that decreased dissolution rate of drug X resulted in a decrease in both C_{max} and AUC_{last} due to slow drug release in the airway fluid (Supplemental Fig. 6).

There are a few limitations to our OI-PBPK model. First, the model does not consider device-related parameters such as device geometry, spray angle, plume size and force, or orifice diameter. However, it does consider critical parameters for drug deposition prediction like aerodynamic particle size distribution, inhalation flow, and inhalation volume. Second, for simplicity, we used a monodisperse particle size distribution rather than a polydisperse to predict regional respiratory deposition of both drugs; however, the latter can be accomplished using a normal or lognormal particle size distribution. Third, though our model considers regional deposition and absorption, it does not do so for each generation of the respiratory tract due to a lack of required physiologic data for each generation. Fifth, the effect, if any, of the excipient on the diameter

of the OID particles other than hygroscopicity, can be addressed using the DF_{scalar}. Further, inclusion of regional thickness to calculate regional apparent permeability can be further tested with regional in vitro permeability experiments for both the test drugs. In addition, once data are available (or curated from the literature), our OI-PBPK model can easily be populated with interindividual variability in physiologic (including the effect of age and sex) or drug-dependent parameters as well as the regional abundances of DMET proteins in the respiratory tract. All these refinements will be important for IVIVE of local and systemic exposure to OID.

In summary, our developed OI-PBPK model was successfully validated using systemic plasma concentrations after OI administration of morphine or nicotine. In addition, we conducted sensitivity analyses to show how various drug or physiologic parameters will impact regional respiratory tract tissue as well as systemic concentrations of OID. We believe, after further validation with additional OID, our OI-PBPK model could be used in the future to predict regional lung tissue and systemic concentration of drugs to optimize OID dosing regimen and evaluate BE of generic OID when systemic drug concentrations are not measurable or are not a good surrogate of the tissue drug concentrations relevant for the PD of the drug.

Acknowledgments

The authors members of the UWPKDAP program for their helpful discussion. and Dr. Sumit Bansal, Dr. Flavia Storelli, Aditya Kumar, and Jinfu Peng for their valuable suggestions on the manuscript. Servier Medical Art (https://smart.servier.com/), BioRender (https://biorender.com/), and Microsoft Office Excel and PowerPoint (https://www.office.com/) were used to create the figures.

Authorship Contributions

Participated in research design: Ladumor, Unadkat.

Conducted experiments: Ladumor.

Performed data analysis: Ladumor, Unadkat.

Wrote or contributed to the writing of the manuscript: Ladumor, Unadkat.

References

Bäckman P, Arora S, Couet W, Forbes B, De Kruijf W, and Paudel A (2018) Advances in experimental and mechanistic computational models to understand pulmonary exposure to inhaled drugs. *Eur J Pharm Sci* **113**:41–52.

Baile EM (1996) The anatomy and physiology of the bronchial circulation. *J Aerosol Med* **9**:1–6.

Boger E, Evans N, Chappell M, Lundqvist A, Ewing P, Wigenborg A, and Fridén M, (2016) Systems Pharmacology Approach for Prediction of Pulmonary and Systemic Pharmacokinetics and Receptor Occupancy of Inhaled Drugs. *CP T Pharmacometrics Syst Pharmacol* **5**:201–210.

Borghardt JM, Weber B, Staab A, and Kloft C (2015) Pharmacometric models for characterizing the pharmacokinetics of orally inhaled drugs. *AAPS J* **17**:853–870.

Bosquillon C (2010) Drug transporters in the lung–do they play a role in the biopharmaceutics of inhaled drugs? *J Pharm Sci* **99**:2240–2255.

Brand P, Meyer T, Häussermann S, Schulte M, Scheuch G, Bernhard T, Sommerauer B, Weber N, and Griese M (2005) Optimum peripheral drug deposition in patients with cystic fibrosis. *J Aerosol Med* **18**:45–54.

Brillault J, De Castro WV, and Couet W (2010) Relative contributions of active mediated transport and passive diffusion of fluoroquinolones with various lipophilicities in a Calu-3 lung epithelial cell model. *Antimicrob Agents Chemother* **54**:543–545.

Chalvatzaki E and Lazaridis M (2018) A dosimetry model of hygroscopic particle growth in the human respiratory tract. *Air Qual Atmos Health* **11**:471–482.

Crowe A and Tan AM (2012) Oral and inhaled corticosteroids: differences in P-glycoprotein (ABCB1) mediated efflux. *Toxicol Appl Pharmacol* **260**:294–302.

Derendorf H, Nave R, Drollmann A, Cerasoli F, and Wurst W (2006) Relevance of pharmacokinetics and pharmacodynamics of inhaled corticosteroids to asthma. *Eur Respir J* **28**:1042–1050.

Dershwitz M, Walsh JL, Morishige RJ, Connors PM, Rubsamen RM, Shafer SL, and Rosow CE (2000) Pharmacokinetics and pharmacodynamics of inhaled versus intravenous morphine in healthy volunteers. *Anesthesiology* **93**:619–628.

Ehrhardt C, Bäckman P, Couet W, Edwards C, Forbes B, Fridén M, Gumbleton M, Hosoya K-I, Kato Y, Nakanishi T et al. (2017) Current progress toward a better understanding of drug disposition within the lungs: summary proceedings of the first workshop on drug transporters in the lungs. *J Pharm Sci* **106**:2234–2244.

Emoto C, Fukuda T, Johnson TN, Neuhoff S, Sadhasivam S, and Vinks AA (2017) Characterization of contributing factors to variability in morphine clearance through PBPK modeling implemented with OCT1 transporter. *CPT Pharmacometrics Syst Pharmacol* **6**:110–119.

Emoto C, Johnson TN, Neuhoff S, Hahn D, Vinks AA, and Fukuda T (2018) PBPK model of morphine incorporating developmental changes in hepatic OCT1 and UGT2B7 proteins to explain the variability in clearances in neonates and small infants. *CPT Pharmacometrics Syst Pharmacol* **7**:464–473.

Eriksson J, Thörn H, Lennernäs H, and Sjögren E (2020) Pulmonary drug absorption and systemic exposure in human: predictions using physiologically based biopharmaceutics modeling. *Eur J Pharm Biopharm* **156**:191–202.

Gaohua L, Wedagedera J, Small BG, Almond L, Romero K, Hermann D, Hanna D, Jamei M, and Gardner I (2015) Development of a multicompartment permeability-limited lung PBPK model and its application in predicting pulmonary pharmacokinetics of antituberculosis drugs. *CPT Pharmacometrics Syst Pharmacol* **4**:605–613.

Gardenhire DS, Burnett D, Strickland S, and Myers T (2017) *Aerosol Delivery Devices for Respiratory Therapists*, American Association for Respiratory Care, Irving.

Gehr P (1994) Annexe A. Anatomy and morphology of the respiratory tract. *Ann ICRP* **24**: 121–166.

Haddrell AE, Davies JF, Miles RE, Reid JP, Dailey LA, and Murnane D (2014) Dynamics of aerosol size during inhalation: hygroscopic growth of commercial nebulizer formulations. *Int J Pharm* **463**:50–61.

Haghnegahdar A, Zhao J, Kozak M, Williamson P, and Feng Y, (2019) Development of a hybrid CFD-P BP K model to predict the transport of xenon gas around a human respiratory system to systemicregions. *Heliyon* **5**:e01461.

Hartung N, and Borghardt JM (2020) A mechanistic framework for a priori pharmacokinetic predictions of orally inhaled drugs. *P LoS Comput Biol* **16**:e1008466.

Hendrickx R, Lamm Bergström E, Janzén DLI, Fridén M, Eriksson U, Grime K, and Ferguson D (2018) Translational model to predict pulmonary pharmacokinetics and efficacy in man for inhaled bronchodilators. *CPT Pharmacometrics Syst Pharmacol* **7**:147–157.

Hintz RJ and Johnson KC (1989) The effect of particle size distribution on dissolution rate and oral absorption. *Int J Pharm* **51**:9–17.

Horvath G, Mendes ES, Schmid N, Schmid A, Conner GE, Salathe M, and Wanner A (2007) The effect of corticosteroids on the disposal of long-acting β2-agonists by airway smooth muscle cells. *J Allergy Clin Immunol* **120**:1103–1109.

Huang W and Isoherranen N (2020) Sampling site has a critical impact on physiologically based pharmacokinetic modeling. *J Pharmacol Exp Ther* **372**:30–45.

ICRP (1995) *ICRP Publication 66: Human Respiratory Tract Model for Radiological Protection*, Elsevier Health Sciences.

Ke AB, Nallani SC, Zhao P, Rostami-Hodjegan A, and Unadkat JD (2012) A PBPK model to predict disposition of CYP3A-metabolized drugs in pregnant women: verification and discerning the site of CYP3A induction. *CPT Pharmacometrics Syst Pharmacol* **1**:e3.

Ke AB, Nallani SC, Zhao P, Rostami-Hodjegan A, Isoherranen N, and Unadkat JD (2013) A physiologically based pharmacokinetic model to predict disposition of CYP2D6 and CYP1A2 metabolized drugs in pregnant women. *Drug Metab Dispos* **41**:801–813.

Ke AB, Nallani SC, Zhao P, Rostami-Hodjegan A, and Unadkat JD (2014) Expansion of a PBPK model to predict disposition in pregnant women of drugs cleared via multiple CYP enzymes, including CYP2B6, CYP2C9 and CYP2C19. *Br J Clin Pharmacol* **77**:554–570.

Kovar L, Selzer D, Britz H, Benowitz N, St Helen G, Kohl Y, Bals R, and Lehr T (2020) Comprehensive parent–metabolite PBPK/PD modeling insights into nicotine replacement therapy strategies. *Clin Pharmacokinet* **59**:1119–1134.

Kuepfer L, Niederalt C, Wendl T, Schlender JF, Willmann S, Lippert J, Block M, Eissing T, and Teutonico D (2016) Applied concepts in PBPK modeling: how to build a PBPK/PD model. *CPT Pharmacometrics Syst Pharmacol* **5**:516–531.

Kumar A, Terakosolphan W, Hassoun M, Vandera K-K, Novicky A, Harvey R, Royall PG, Bicer EM, Eriksson J, Edwards K et al. (2017) A biocompatible synthetic lung fluid based on human respiratory tract lining fluid composition. *Pharm Res* **34**:2454–2465.

Ladumor MK, Bhatt DK, Gaedigk A, Sharma S, Thakur A, Pearce RE, Leeder JS, Bolger MB, Singh S, and Prasad B (2019a) Ontogeny of hepatic sulfotransferases and prediction of age-dependent fractional contribution of sulfation in acetaminophen metabolism. *Drug Metab Dispos* **47**:818–831.

Ladumor MK, Thakur A, Sharma S, Rachapally A, Mishra S, Bobe P, Rao VK, Pammi P, Kangne H, Levi D et al. (2019b) A repository of protein abundance data of drug metabolizing enzymes and transporters for applications in physiologically based pharmacokinetic (PBPK) modelling and simulation. *Sci Rep* **9**:9709.

Melillo N, Grandoni S, Cesari N, Brogin G, Puccini P, and Magni P (2020) Inter-compound and intra-compound global sensitivity analysis of a physiological model for pulmonary absorption of inhaled compounds. *AAPS J* **22**:116.

Miller NA, Graves RH, Edwards CD, Amour A, Taylor E, Robb O, O'Brien B, Patel A, Harrell AW, and Hessel EM (2022) Physiologically Based Pharmacokinetic Modelling of Inhaled Nemiralisib: Mechanistic Components for Pulmonary Absorption, Systemic Distribution, and Oral Absorption. *Clin Pharmacokinet* **61**:281–293.

Miller-Larsson A, Mattsson H, Hjertberg E, Dahlbäck M, Tunek A, and Brattsand R (1998) Reversible fatty acid conjugation of budesonide. Novel mechanism for prolonged retention of topically applied steroid in airway tissue. *Drug Metab Dispos* **26**:623–630.

Mobley C and Hochhaus G (2001) Methods used to assess pulmonary deposition and absorption of drugs. *Drug Discov Today* **6**:367–375.

Newman B and Witzmann K (2020) Addressing the regulatory and scientific challenges with generic orally inhaled drug products. *Pharmaceut Med* **34**:93–102.

Oesch F, Fabian E, and Landsiedel R (2019) Xenobiotica-metabolizing enzymes in the lung of experimental animals, man and in human lung models. *Arch Toxicol* **93**:3419–3489.

Olsson B, Bondesson E, Borgström L, Edsbäcker S, Eirefelt S, Ekelund K, Gustavsson L, and Hegelund-Myrbäck T (2011) Pulmonary drug metabolism, clearance, and absorption, in *Controlled Pulmonary Drug Delivery* (Smyth HDC and Hickey AJ eds) pp 21–50, Springer.

Paquet F, Etherington G, Bailey MR, Leggett RW, Lipsztein J, Bolch W, Eckerman KF, and Harrison JD; ICRP (2015) ICRP publication 130: occupational intakes of radionuclides: part 1. *Ann ICRP* **44**:5–188.

Po HN and Senozan N (2001) The Henderson-Hasselbalch equation: its history and limitations. *J Chem Educ* **78**:1499.

Sadiq MW, Holz O, Ellinghusen BD, Faulenbach C, Müller M, Badorrek P, Eriksson UG, Fridén M, Stomilovic S, Lundqvist AJ et al. (2021) Lung pharmacokinetics of inhaled and systemic drugs: A clinical evaluation. *Br J Pharmacol* **178**:4440–4451.

Sakamoto A, Matsumaru T, Yamamura N, Uchida Y, Tachikawa M, Ohtsuki S, and Terasaki T (2013) Quantitative expression of human drug transporter proteins in lung tissues: analysis of

regional, gender, and interindividual differences by liquid chromatography-tandem mass spectrometry. *J Pharm Sci* **102**:3395–3406.
Schroeter JD, Musante CJ, Hwang D, Burton R, Guilmette R, and Martonen TB (2001) Hygroscopic growth and deposition of inhaled secondary cigarette smoke in human nasal pathways. *Aerosol Sci Technol* **34**:137–143.
Schuster J, Rubsamen R, Lloyd P, and Lloyd J (1997) The AERX aerosol delivery system. *Pharm Res* **14**:354–357.
Shao J, Wang Y, and Hochhaus G (2021) Semi-mechanistic P K/P D model to assess pulmonary targeting of beclomethasone dipropionate and its active metabolite. *Eur J Pharm Sci* **159**:105699
Somers GI, Lindsay N, Lowdon BM, Jones AE, Freathy C, Ho S, Woodrooffe AJ, Bayliss MK, and Manchee GR (2007) A comparison of the expression and metabolizing activities of phase I and II enzymes in freshly isolated human lung parenchymal cells and cryopreserved human hepatocytes. *Drug Metab Dispos* **35**:1797–1805.
Würthwein G and Rohdewald P (1990) Activation of beclomethasone dipropionate by hydrolysis to beclomethasone-17-monopropionate. *Biopharm Drug Dispos* **11**:381–394.
Yu J–Y and Rosania GR (2010) Cell-based multiscale computational modeling of small molecule absorption and retention in the lungs. *Pharm Res* **27**:457–467.
Zhang Z, Imperial MZ, Patilea-Vrana GI, Wedagedera J, Gaohua L, and Unadkat JD (2017) Development of a novel maternal-fetal physiologically based pharmacokinetic model I: insights into factors that determine fetal drug exposure through simulations and sensitivity analyses. *Drug Metab Dispos* **45**:920–938.
Zhang Z and Unadkat JD (2017) Development of a novel maternal-fetal physiologically based pharmacokinetic model II: verification of the model for passive placental permeability drugs. *Drug Metab Dispos* **45**:939–946.
Zhang JY, Wang Y, and Prakash C (2006) Xenobiotic-metabolizing enzymes in human lung. *Curr Drug Metab* **7**:939–948.
Zhao L, Seo P, and Lionberger R (2019) Current scientific considerations to verify physiologically-based pharmacokinetic models and their implications for locally acting products. *CPT Pharmacometrics Syst Pharmacol* **8**:347–351.

Address correspondence to: Jashvant D. Unadkat, Department of Pharmaceutics, School of Pharmacy, University of Washington, Box 357610, Seattle, WA 98195. E-mail: jash@uw.edu

Supplemental Data

Title:

Predicting Regional Respiratory Tissue and Systemic Concentrations of Orally Inhaled Drugs through a Novel PBPK Model

Authors:

Mayur K. Ladumor and Jashvant D. Unadkat

Affiliation:

Department of Pharmaceutics, School of Pharmacy, University of Washington, Seattle, WA (M.K.L., J.D.U.)

Journal Title:

Drug Metabolism and Disposition

Manuscript Number:

DMD-AR-2021-000789

Supplemental Method

Drug Deposition Model. The regional dose exposure for each respiratory tract region was calculated by multiplying the regional deposition efficiency (DE, dimensionless; sometimes referred to as deposition fraction, DF) with the overall OI dose (Eq. 1)

$$\mathrm{Dose_{region}} = \mathrm{DE_{region}} \times \mathrm{OI\ dose} \tag{1}$$

During both the inhalation (inh) and exhalation (exh) cycles, each region acts as a filter (N=7 for the OI route) of the drug particles/droplets that flow through the region. The total and regional DE in the extrathoracic (ET2, oral passage), bronchial (BB), bronchiolar (bb), and alveolar (AL) regions were calculated by adding the DE in each filter during inh and exh cycle (Eqs. 2-7).

$$\mathrm{DE_{ET2}} = \mathrm{DE_{1,inh}} + \mathrm{DE_{7,exh}} \tag{2}$$

$$\mathrm{DE_{BB}} = \mathrm{DE_{2,inh}} + \mathrm{DE_{6,exh}} \tag{3}$$

$$\mathrm{DE_{bb}} = \mathrm{DE_{3,inh}} + \mathrm{DE_{5,exh}} \tag{4}$$

$$\mathrm{DE_{AL}} = \mathrm{DE_{4,inh\ and\ exh}} \tag{5}$$

$$\mathrm{DE_{total}} = \mathrm{DE_{ET2}} + \mathrm{DE_{BB}} + \mathrm{DE_{bb}} + \mathrm{DE_{AL}} \tag{6}$$

$$\mathrm{f_{exhaled}} = 1 - \mathrm{DE_{total}} \tag{7}$$

where $f_{exhaled}$ is fraction exhaled.

The DE of each filter was calculated using the ICRP 66 deposition model (Eq. 8) as follows.

$$\mathrm{DE_j} = \mathrm{DE_{j-1}} \cdot \eta_j \cdot \xi_j \cdot \left(\frac{1}{\eta_{j-1}} - 1\right), \quad \text{for j} = 1 \text{ to } 7 \tag{8}$$

where, j denotes the number of filters connected in series. η_j is the total filtration efficiency (dimensionless) of the j^{th} filter, i.e. the fraction of drug particles that enter and are deposited in the filter. ξ_j is a dimensionless factor that accounts for the different air volumes that pass through the filter.

The η_j for each filter was calculated using Eq. 9 as described below.

$$\eta_j = \left(\eta_{ae,j}^2 + \eta_{th,j}^2\right)^{1/2} \tag{9}$$

where, $\eta_{ae,j}$ and $\eta_{th,j}$ denote the aerodynamic (accounting for impaction and gravitational settling) and thermodynamic (accounting for particle diffusion by Brownian motion) filtration efficiencies (dimensionless), respectively and calculated as indicated in Tables S1 and S2.

ξ_j for each filter was calculated using Eq. 10 as described below.

$$\xi_j = \frac{\phi_j}{\phi_{j-1}} \quad (10)$$

where ϕ_j is the volumetric fraction (dimensionless) calculated by the cumulative volume of the preceding filters as indicated in Table S3.

To determine DE for the first filter (DE_1), prefiltration efficiency (η_0) at an imaginary prefilter (this filter reflects the potential loss of particles/droplets before entering the mouth) was calculated using Eq. 11.

$$\eta_0 = (1 - \eta_I) \quad (11)$$

where η_I is defined as inhalability (Eq. 12), defined as the fraction of drug particles in ambient air that enter the mouth before inhalation.

$$\eta_I = 1 - 0.5\,(1 - [7.6 \times 10^{-4}\ d_{ae}^{2.8} + 1]^{-1}) + 1.0\ \times 10^{-5}\ U^{2.75} \exp\,(0.055 \cdot d_{ae}) \quad (12)$$

where d_{ae} stands for aerodynamic diameter (μm), which is defined as the "diameter of unit density (1 g/mL) sphere that has same terminal settling velocity in air as the particle of interest", and U denotes windspeed (m/s), which is defined as the rate at which air enters the respiratory tract via the mouth passage.

In order to calculate η_{th}, thermodynamic diameter (d_{th} (μm) is defined as "diameter of a spherical particle that has the same diffusion coefficient (D; Eq. 15) in air as the particle of interest") was determined using Eq. 13.

$$d_{th} = d_{ae} \cdot \sqrt{\frac{\chi \cdot \rho_0}{\rho} \cdot \frac{C(d_{ae})}{C(d_{th})}} \quad (13)$$

where, ρ_0 and ρ are the unit density (1 g/mL) and drug density (g/mL), respectively; χ is the particle shape factor (dimensionless); $C(d_{ae})$ or $C(d_{th})$ is dimensionless slip correction factor for d_{ae} and d_{th} (Eq. 12), which is defined as "particle slip caused by the relative velocity of gas molecules at the particle surface".

$$C(d) = 1 + \frac{\lambda}{d} \cdot \left[2.514 + 0.800 \exp\left(-0.55\ \cdot \frac{d}{\lambda}\right)\right] \quad (14)$$

where, λ (μm) is a mean free path of the air molecules at 37°C, 100% relative humidity and 76 cm Hg atmospheric pressure. d is a diameter (d_{ae} or d_{th}). Convergence of Eq. 13 and 14 was achieved by using the initial setting such as $d_{th} = d_{ae} \cdot \sqrt{\chi/\rho}$.

$$D = \frac{k_B \cdot T \cdot C(d_{th})}{3 \cdot \pi \cdot \mu_{air} \cdot d_{th}} \quad (15)$$

where, k_B is the Boltzmann constant, T is the absolute body temperature in Kelvin and μ_{air} is the viscosity of air.

The hygroscopic growth of aerosol was integrated using Eq. 16 and 17, and the resulting new values of $d_{ae,j}$ and D_j in each regional filter j were substituted for the d_{ae} and D in Tables S1 and S2.

$$d_{ae,j} = d_{ae,\infty} - \left(d_{ae,\infty} - d_{ae,0}\right) \cdot \left(\exp\left[\frac{-\left(10 \cdot t_{r,j}\right)^{0.55}}{d_{ae,0}}\right]\right)^{0.6} \quad (16)$$

$$D_j = D_0 - \left(\frac{d_{ae,j} - d_{ae,0}}{d_{ae,\infty} - d_{ae}}\right) \cdot (D_0 - D_\infty) \quad (17)$$

where $t_{r,j}$ is the residence time in regional filter j (Eqs. 20-23); $d_{ae,0}$ and D_0 are the initial values of d_{ae} and D; $d_{ae,\infty}$ and D_∞ are the equilibrium values of d_{ae} and D, respectively, as determined by hygroscopic growth factor ($f_{hyg,}$ this is generally between 2-4-fold at equilibrium) using Eq. 16 and 17.

$$d_{ae,\infty} = d_{ae,0} \cdot f_{hyg} \quad (18)$$

$$D_\infty = D_0 / f_{hyg} \quad (19)$$

Residence time in second (s) for ET2, BB, bb and AL was calculated using Eqs. 20-23 considering the regional (n) dead space volume ($V_{D,n}$), tidal or inhalation volume (V), volumetric or inhalation flow rate (Q) and functional residual capacity (FRC).

$$t_{r,ET2} = 0.1 \quad (20)$$

$$t_{r,BB} = \frac{V_{D,BB}}{Q} \cdot \left(1 + \frac{0.5 \cdot V}{FRC}\right) \quad (21)$$

$$t_{r,bb} = \frac{V_{D,bb}}{Q} \cdot \left(1 + \frac{0.5 \cdot V}{FRC}\right) \quad (22)$$

$$t_{r,AL} = \frac{V - V_{D,ET} - \left[V_{D,BB} + V_{D,bb}\right] \cdot \left(1 + \frac{V}{FRC}\right)}{Q} \quad (23)$$

Drug Absorption Model. The mass balance equations for the regional respiratory absorption, lymphatic and systemic model are shown below.

ELF or Airway Liquid Compartment. The mass balance in the ELF compartment can be described using the following differential equation Eq. 24 and 25.

$$\frac{dA_{ud,n}}{dt} = k_{t,n+1} \cdot A_{ud,n+1} - k_{t,n} \cdot A_{un,n} - K_{dis,n} \cdot A_{ud,n} \cdot \left(C_{s,n} - Cu_{dis,n}\right) \quad (24)$$

$$\frac{dC_{dis,n}}{dt} = \frac{1}{V_{F,n}} \cdot \left[k_{t,n+1} \cdot A_{dis,n+1} \cdot V_{F,n} - k_{t,n} \cdot A_{dis,n} \cdot V_{F,n} + K_{dis,n} \cdot A_{ud,n} \cdot \left(C_{s,n} - Cu_{dis,n}\right) - k_{deg,n} \cdot Cu_{dis,n} \cdot V_{F,n} - PS_n \cdot \left(Cu_{dis,n} \cdot fui_{F,n} - Cu_{E,n} \cdot fui_{E,n}\right) - CL_{inf,F-E} \cdot Cu_{dis,n} + CL_{eff,E-F} \cdot Cu_{E,n}\right] \quad (25)$$

where $A_{ud,n}$ is the undissolved drug amount in the n^{th} ELF compartment of the respiratory tract; $k_{t,n}$ represent the transit rate constants in the n^{th} compartment; $K_{dis,n}$ represents the dissolution rate constant of the undissolved drug amount in the n^{th} compartment (Eq. 26); $C_{s,n}$ is drug solubility in the n^{th} compartment; $V_{F,n}$ represent the ELF volume of the n^{th} compartment; $Cu_{dis,n}$ denotes the unbound dissolved drug concentration in the n^{th} ELF compartment; subscript F, E and n denote ELF compartment, epithelial compartment and region of the respiratory compartment, respectively; $k_{deg,n}$ is the first-order degradation rate constant in the n^{th} ELF compartment; fui denote fraction of unionized drug; PS, permeability-surface area product; $CL_{inf,F-E}$, active influx transporter-mediated drug clearance from ELF to epithelial direction; $CL_{eff,E-F}$, active efflux transporter-mediated drug clearance from epithelial to ELF direction.

Dissolution rate constant. $K_{dis,n}$ or z-factor was determined by Hintz - Johnson model (Hintz and Johnson, 1989) as shown in Eq. 26.

$$K_{dis,n} = \frac{3 \cdot D}{\rho \cdot r \cdot h} \quad (26)$$

where r is the particle radius ($r = d_e/2$; d_e is equivalent volume diameter and was calculated from d_{ae} (Eq. 27)); h is the diffusion layer thickness (h = r if r < 30 μm, otherwise h = 30 μm); D was calculated using Eq. 15 considering the viscosity of simulated lung lining fluid.

$$d_e = d_{ae} \cdot \sqrt{\frac{\chi \cdot \rho_0}{\rho} \cdot \frac{C(d_{ae})}{C(d_e)}} \quad (27)$$

where d_e was converged as described in Eq. 13 and 14 and $C(d_e)$ was calculated according to Eq. 14.

Fraction of unionized drug. fui values for the ELF, epithelial, subepithelial, and blood compartments of the regional respiratory tract were determined by the Henderson-Hasselbalch equation (Po and Senozan, 2001) using pH value of the regional compartment and drug acid dissociation constant (pK_a) data (Eqs. 28-33).

$$fui = 1 \text{ for neutral drug} \quad (28)$$

$$fui = 1/\left[1 + \left(10^{pH - pK_a}\right)\right] \text{ for monoprotic acid drug} \quad (29)$$

$$fui = 1/\left[1 + \left(10^{pH - pK_{a1}} + 10^{2 \cdot pH - pK_{a1} - pK_{a2}}\right)\right] \text{ for diprotic acid } (pK_{a1} < pK_{a2}) \quad (30)$$

$$\mathrm{fui} = 1/[1 + (10^{\mathrm{pK_a - pH}})] \text{ for monoprotic base drug} \quad (31)$$

$$\mathrm{fui} = 1/[1 + (10^{\mathrm{pK_{a2} - pH}} + 10^{\mathrm{pK_{a1} + pK_{a2} - 2 \cdot pH}})] \text{ for diprotic base } (\mathrm{pK_{a1}} < \mathrm{pK_{a2}}) \quad (32)$$

$$\mathrm{fui} = 1/[1 + (10^{\mathrm{pK_{a,base} - pH}} + 10^{\mathrm{pH - pK_{a,acid}}})] \text{ for zwitterion drug} \quad (33)$$

Fraction of unbound drug. If experimental fu values are not available, fu for the epithelial and subepithelial compartments of the regional respiratory tract was calculated using the fraction unbound in plasma (fu_{plasma}), the tissue to plasma partition coefficient ($Kp_{tissue\text{-}pls}$; Eq. 35) and the interstitial to plasma partition coefficient ($Kp_{int\text{-}pls}$; Eqs. 36 and 38) (Schmitt et al., 2008). Lung includes the BB, bb and AL regions. The tissue composition of the ET2 region was assumed to be the same as lung, so the Kp of the ET2 region was identical to the lung tissue.

$$\mathrm{fu_{F,n}} = 1 \quad (34)$$

$$\mathrm{fu_{E,n}} = \mathrm{fu_{plasma}}/\mathrm{Kp_{tissue-pls}} \quad (35)$$

$$\mathrm{fu_{S,n}} = \mathrm{fu_{plasma}}/\mathrm{Kp_{int-pls}} \quad (36)$$

$$\mathrm{fu_{B,n}} = \mathrm{fu_{plasma}}/\mathrm{BP} \quad (37)$$

$$\mathrm{Kp_{int-pls}} = (\mathrm{f_{water,int}} + \text{protein ratio} \cdot (1/(\mathrm{fu_{plasma}} - \mathrm{f_{water,plasma}}))) \cdot \mathrm{fu_{plasma}} \quad (38)$$

Membrane permeability. Apical epithelial membrane permeability or the permeability surface area product (PS) between ELF and epithelial compartment was calculated for each region using the apparent permeability ($P_{app,\ calu\text{-}3}$) obtained from the *in vitro* bronchial epithelial calu-3 model and the surface area (SA) of each respiratory tract region (Eq. 39). To calculate regional P_{app} (Eq. 40), $P_{app,\ calu\text{-}3}$ was then corrected by regional membrane thickness scalar (RT) through thickness, h_{mem}, of the epithelial compartments of BB region and other regions of the respiratory tract (Eq. 41). For the purpose of making the model more general, we used the linear regression model (Eq. 42, R^2 =0.93) for $P_{app,\ calu\text{-}3}$ developed by Brillault and colleagues (Brillault et al., 2010). This model (Eq. 42) is based on *in vitro* $P_{app,\ calu\text{-}3}$ of fluoroquinolones compounds in the presence of a P-glycoprotein (P-gp) inhibitor such as valspodar (PSC-833) and the partition coefficients between octanol and a pH 7.4 buffered solution (logD).

$$\mathrm{PS_n} = \mathrm{P_{app,n}} \cdot \mathrm{SA_n} \quad (39)$$

$$\mathrm{P_{app,n}} = \mathrm{RT_n} \cdot \mathrm{P_{app,calu-3}} \quad (40)$$

$$\mathrm{RT_n} = \frac{\mathrm{h_{mem,BB}}}{\mathrm{h_{mem,n}}} \quad (41)$$

$$\mathrm{P_{app,calu-3}}\ (10^{-6}\ \mathrm{cm/s}) = 6.1 \cdot \mathrm{logD} + 7.5 \quad (42)$$

Epithelial or Intracellular Compartment. The mass balance in the epithelial compartment can be described using the following differential Eq. 43.

$$\frac{dC_{E,n}}{dt} = \frac{1}{V_{E,n}} \cdot \left[PS_n \cdot \left(Cu_{dis,n} \cdot\ fui_{F,n} - Cu_{E,n} \cdot\ fui_{E,n}\right) + CL_{inf,F-E} \cdot Cu_{dis,n} - CL_{eff,E-F} \cdot Cu_{E,n} - PS_n \cdot \left(Cu_{E,n} \cdot\ fui_{E,n} - Cu_{S,n} \cdot\ fui_{S,n}\right) + CL_{inf,S-E} \cdot Cu_{S,n} - CL_{eff,E-S} \cdot Cu_{E,n} - CL_{int,met,n} \cdot Cu_{E,n} - \left(k_{on,n} \cdot Cu_{E,n} \cdot FA - k_{off,n} \cdot C_{conj,E,n}\right) \cdot V_{E,n}\right] \quad (43)$$

where V, Cu, and Q_B denote the volume, unbound drug concentration and blood flow of the tissue, respectively. PS and fui are permeability surface area product and fraction of unionized drug, respectively. $CL_{int,met}$ is intrinsic clearance of drug mediated by metabolism. k_{on} and k_{off} are the second order association and first order dissociation rate constants for tissue retention, respectively. Subscript E, S and n denote epithelial compartment, subepithelial compartment and region of the respiratory compartment, respectively. $CL_{inf,F-E}$, active influx transporter-mediated drug clearance from ELF to epithelial direction; $CL_{eff,E-F}$, active efflux transporter-mediated drug clearance from epithelial to ELF direction; $CL_{inf,S-E}$, active influx transporter-mediated drug clearance from subepithelial to epithelial direction; $CL_{eff,E-S}$, active efflux transporter-mediated drug clearance from epithelial to subepithelial direction; FA, fatty acid concentration.

Subepithelial or Interstitial Compartment. The mass balance in subepithelial compartment can be described using the following differential Eq. 44.

$$\frac{dC_{S,n}}{dt} = \frac{1}{V_{S,n}} \cdot \left[PS_n \cdot \left(Cu_{E,n} \cdot\ fui_{E,n} - Cu_{S,n} \cdot\ fui_{S,n}\right) - PS_n \cdot \left(Cu_{S,n} \cdot\ fui_{S,n} - Cu_{B,n} \cdot\ fui_{B,n}\right) - CL_{inf,E-S} \cdot Cu_{S,n} + CL_{eff,S-E} \cdot Cu_{E,n} + Q_{L,n} \cdot Cu_{S,n}\right] \quad (44)$$

where V, Cu, Q_B and Q_L denote the volume, unbound drug concentration, blood flow and lymph flow of the tissue, respectively. PS and fui are permeability surface area product and fraction of unionized drug, respectively. Subscript E, S and n denote epithelial compartment, subepithelial compartment and region of the respiratory compartment, respectively; $CL_{inf,E-S}$, active influx transporter-mediated drug clearance from epithelial to subepithelial direction; $CL_{eff,S-E}$, active efflux transporter-mediated drug clearance from subepithelial to epithelial direction.

Blood or Vascular Compartment. The mass balance in the blood compartment of ET2, BB and bb regions can be described using the following differential Eq. 45.

$$\frac{dC_{B,n}}{dt} = \frac{1}{V_{B,n}} \cdot \left[PS_n \cdot \left(Cu_{S,n} \cdot\ fui_{S,n} - Cu_{B,n} \cdot\ fui_{B,n}\right) + Q_{B,n} \cdot C_{ab,n} - \left(Q_{B,n} - Q_{L,n}\right) \cdot C_{B,n}\right] \quad (45)$$

The mass balance in the blood compartment of AL region can be described using the following differential Eq. 46.

$$\frac{dC_{B,AL}}{dt} = \frac{1}{V_{B,AL}} \cdot \left[PS_{AL} \cdot \left(Cu_{S,AL} \cdot\ fui_{S,AL} - Cu_{B,AL} \cdot\ fui_{B,AL}\right) + Q_{B,AL} \cdot C_{vb} - \left(Q_{B,AL} - Q_{L,AL}\right) \cdot C_{B,AL}\right] \quad (46)$$

where V, Cu, Q_B and Q_L denote the volume, unbound drug concentration, blood flow and lymph flow of the tissue, respectively. PS and fui are permeability surface area product and fraction of unionized drug, respectively. Subscript S and B denote subepithelial compartment and blood compartment, respectively.

Lymph node compartment (LN). The mass balance in the lymph node compartment of AL region can be described using the following differential Eq. 47.

$$\frac{dC_{LN}}{dt} = \frac{1}{V_{LN}} \cdot \left[Q_{L,ET2} \cdot C_{S,ET2} + Q_{L,BB} \cdot C_{S,BB} + Q_{L,bb} \cdot C_{S,bb} + Q_{L,AL} \cdot C_{S,AL} - Q_{L,LN} \cdot C_{LN}\right] \quad (47)$$

where V, C and Q_L denote the volume, concentration and lymph flow of the tissue, respectively. LN, ET2, BB, bb, AL, S and B denote the lymph node, extrathoracic (oral passage), bronchial, bronchiolar, alveolar, subepithelial and blood, respectively.

Whole-body PBPK model. The mass balance equations for the whole-body PBPK model are shown below (Eqs. 48-54).

Arterial blood compartment (ab).

$$\frac{dC_{ab}}{dt} = \frac{1}{V_{ab}} \cdot \left[\left(Q_{B,AL} - Q_{L,AL}\right) \cdot C_{B,AL} - Q_{B,ET2} \cdot C_{ab} - Q_{B,BB} \cdot C_{ab} - Q_{B,bb} \cdot C_{ab} - Q_{B,adipose} \cdot C_{ab} - Q_{B,bone} \cdot C_{ab} - Q_{B,brain} \cdot C_{ab} - Q_{B,heart} \cdot C_{ab} - Q_{B,kidney} \cdot C_{ab} - Q_{B,muscle} \cdot C_{ab} - Q_{B,skin} \cdot C_{ab} - \left(Q_{B,liver} - Q_{B,gut} - Q_{B,spleen} - Q_{B,pancreas}\right) \cdot C_{ab} - Q_{B,gut} \cdot C_{ab} - Q_{B,spleen} \cdot C_{ab} - Q_{B,pancreas} \cdot C_{ab}\right] \quad (48)$$

where V, C, Q_B and Q_L denote the volume, concentration, blood flow and lymph flow of the tissue, respectively. ab, ET2, BB, bb, and AL denote the arterial blood, extrathoracic (oral passage), bronchial, bronchiolar, and alveolar, respectively.

Venous blood compartment (vb).

$$\frac{dC_{vb}}{dt} = \frac{1}{V_{vb}} \cdot \left[\left(Q_{B,ET} - Q_{L,ET}\right) \cdot C_{B,ET} + \left(Q_{BB} - Q_{L,BB}\right) \cdot C_{B,BB} + \left(Q_{bb} - Q_{L,bb}\right) \cdot C_{B,bb} - Q_{B,AL} \cdot C_{vb} + Q_{L,LN} \cdot C_{LN} + Q_{B,adipose} \cdot \frac{C_{adipose}}{Kp_{adipose/BP}} + Q_{B,bone} \cdot \frac{C_{bone}}{Kp_{bone/BP}} + Q_{B,brain} \cdot \frac{C_{brain}}{Kp_{brain/BP}} + Q_{B,heart} \cdot \frac{C_{heart}}{Kp_{heart/BP}} + Q_{B,kidney} \cdot \frac{C_{kidney}}{Kp_{kidney/BP}} + Q_{B,muscle} \cdot \frac{C_{muscle}}{Kp_{muscle/BP}} + Q_{B,skin} \cdot \frac{C_{skin}}{Kp_{skin/BP}} + Q_{B,liver} \cdot \frac{C_{liver}}{Kp_{liver/BP}} - CL_{renal} \cdot fu_B \cdot C_{vb} + Q_{B,forearm} \cdot C_{forearm}\right] \quad (49)$$

where V, C, Q_B and Q_L denote the volume, concentration, blood flow and lymph flow of the tissue, respectively. C_{vb} denotes the venous blood concentration, Kp denotes the tissue-to-plasma partition coefficient of the tissue, and fu_B denotes the fraction unbound in blood. ET2, BB, bb, and AL denote the extrathoracic (oral passage), bronchial, bronchiolar, and alveolar, respectively.

Non-eliminating tissue.

$$\frac{dC_{tissue}}{dt} = \frac{1}{V_{tissue}} \cdot \left[Q_{B,tissue} \cdot \left(C_{ab} - \frac{C_{tissue}}{Kp_{tissue}/BP} \right) \right] \quad (50)$$

where V_{tissue}, C_{tissue}, and $Q_{B,tissue}$ denote the volume, concentration, and blood flow of the tissue, respectively. C_{ab}, Kp_{tissue}, and BP denote the arterial blood concentration, tissue-to-plasma partition coefficient, and blood-to-plasma concentration ratio, respectively.

Eliminating tissue (liver).

$$\frac{dC_{liver,B}}{dt} = \frac{1}{V_{liver}} \cdot \left[\left(Q_{B,liver} - Q_{B,gut} - Q_{B,spleen} - Q_{B,pancreas} \right) \cdot C_{ab} + Q_{B,gut} \cdot \frac{C_{gut}}{Kp_{gut}/BP} + Q_{spleen} \cdot \frac{C_{spleen}}{Kp_{spleen}/BP} + Q_{B,pancreas} \cdot \frac{C_{pancreas}}{Kp_{pancreas}/BP} - Q_{B,liver} \cdot C_{liver,B} - PS_{B-IS\ or\ IS-B} \cdot \left(Cu_{liver,B} \cdot fui_{liver,B} - Cu_{liver,IS} \cdot fui_{liver,IS} \right) \right] \quad (51)$$

$$\frac{dC_{liver,IS}}{dt} = \frac{1}{V_{liver,IS}} \cdot \left[PS_{B-IS\ or\ IS-B} \cdot \left(Cu_{liver,B} \cdot fui_{liver,B} - Cu_{liver,IS} \cdot fui_{liver,IS} \right) + PS_{IS-IC\ or\ IC-IS} \cdot \left(Cu_{liver,IC} \cdot fui_{liver,IC} - Cu_{liver,IS} \cdot fui_{liver,IS} \right) - CL_{inf,IS-IC} \cdot Cu_{liver,IS} + CL_{eff,IC-IS} \cdot Cu_{liver,IC} \right] \quad (52)$$

$$\frac{dC_{liver,IC}}{dt} = \frac{1}{V_{liver,IC}} \cdot \left[PS_{IS-IC\ or\ IC-IS} \cdot \left(Cu_{liver,IS} \cdot fui_{liver,IS} - Cu_{liver,IC} \cdot fui_{liver,IC} \right) + CL_{inf,IS-IC} \cdot Cu_{liver,IS} - CL_{eff,IC-IS} \cdot Cu_{liver,IC} - CL_{int,H} \cdot Cu_{liver,IC} \right] \quad (53)$$

Subscript B, IS and IC denote blood, interstitial and intracellular compartments, respectively. where V, Cu and Q_B denote the volume, unbound drug concentration and blood flow of the tissue, respectively. PS and fui are permeability surface area product and fraction of unionized drug, respectively. CL_{inf} and CL_{eff} are active influx and efflux transporter-mediated drug clearance, respectively. C_{ab}, Kp_{tissue}, and BP denote the arterial blood concentration, tissue-to-plasma partition coefficient, and blood-to-plasma concentration ratio, respectively. $CL_{int,H}$, denotes the intrinsic hepatic drug metabolic clearance.

Forearm (peripheral sampling) compartment.

$$\frac{dC_{forearm}}{dt} = \frac{1}{V_{forearm}} \cdot \left[Q_{B,anastomoses} \cdot C_{ab} + Q_{B,forearm\ muscle} \cdot \frac{C_{forearm\ muscle}}{Kp_{muscle/BP}} + Q_{B,forearm_{skin}} \cdot \frac{C_{forearm\ skin}}{Kp_{skin/BP}} + Q_{B,forearm\ adipose} \cdot \frac{C_{forearm\ adipose}}{Kp_{adipose/BP}} - Q_{B,forearm} \cdot C_{forearm}\right] \quad (54)$$

where V, C, and Q_B denote the volume, concentration, and blood flow of the tissue, respectively. C_{ab}, Kp_{tissue}, and BP denote the arterial blood concentration, tissue-to-plasma partition coefficient, and blood-to-plasma concentration ratio, respectively.

***In vitro* to *in vivo* extrapolation (IVIVE).** Drug metabolizing enzyme or transporter (DMET) mediated *in vivo* intrinsic clearance in reference organ such as the liver ($CL_{int,ref\ organ}$; in L/h unit) can be determined by *in vitro* intrinsic clearance ($CL_{int,in\ vitro}$; in μL/min/mg subcellular fraction protein or μL/min/number of cells) or by the *vitro* unbound Michaelis-Menten kinetics for the enzyme (maximum enzymatic reaction rate (V_{max})/ substrate affinity (K_m)) or transporter (maximum transport rate (J_{max})/K_m)) through IVIVE (Eqs. 55-58).

$$CL_{int,ref\ organ} = CL_{int,in\ vitro} \times PSF \times organ\ weight \times 60 \times 10^{-6} \quad (55)$$

$$CL_{int,RT} = CL_{int,ref\ organ} \times RA_{RT} \quad (56)$$

$$RA_{RT} = \frac{A_{protein,RT}}{A_{protein,ref\ organ}} \quad (57)$$

$$A_{protein,organ} = A_{protein,subcellular\ fraction} \times PSF \times Organ\ weight \times 10^{-6} \quad (58)$$

where PSF is the physiological scaling factor (yield of the subcellular fraction from whole organ (in mg subcellular fraction protein/g organ or number of cells/g of organ)); organ weight is the subject's organ weight (in g); ref organ, RT and RA denote the reference organ (e.g. liver), respiratory tract regions (ET2, BB, bb and AL) and relative protein abundance, respectively; $A_{protein,organ}$ is the protein abundance of DMET per whole organ (in μmol unit); $A_{protein,subcellular}$ is the protein abundance of DMET per subcellular fraction of organ (in pmol/mg subcellular fraction protein unit); 60×10^{-6} and 10^{-6} are unit conversion factors to convert the $CL_{int,ref\ organ}$ to L/h and $A_{protein,organ}$ to μmol, respectively.

Supplemental Tables

Table S1. Algebraic expressions for aerodynamic filtration efficiency in the ICRP 66 deposition model (ICRP, 1995).

Aerodynamic filtration efficiency ($\eta_{ae} = 1-\exp(-aR^P)$)					
Phase	**Filter (j)**	**Region**	**a**	**R**	**P**
Inhalation	1	ET_2[$]	$1.1 \cdot 10^{-4}$	$d_{ae}^2 \cdot (Q \cdot SF_{BB}^3)^{0.6} \cdot (V \cdot SF_{BB}^2)^{-0.2}$	1.4
	2	BB	$4.08 \cdot 10^{-6}$	$d_{ae}^2 \cdot Q \cdot SF_{BB}^{2.3}$	1.152
	3	bb	0.1147	$(0.056 + t_{r,bb}^{1.5}) \cdot d_{ae}^{\ tr,bb\text{^}-0.25}$	1.173
	4	AL	$0.146 \cdot SF_{AL}^{0.98}$	$d_{ae}^2 \cdot t_{r,AL}$	0.6495
Exhalation	5	bb	0.1147	$(0.056 + t_{r,bb}^{1.5}) \cdot d_{ae}^{\ tr,bb\text{^}-0.25}$	1.173
	6	BB	$2.04 \cdot 10^{-6}$	$d_{ae}^2 \cdot Q \cdot SF_{BB}^{2.3}$	1.152
	7	ET_2[$]	$1.1 \cdot 10^{-4}$	$d_{ae}^2 \cdot (Q \cdot SF_{BB}^3)^{0.6} \cdot (V \cdot SF_{BB}^2)^{-0.2}$	1.4

a and P are constants and R is a parameter, which is drug- and system-dependent. a, P and R were obtained from ICRP 66 deposition model (ICRP, 1995). ET2, extrathoracic (oral passage); BB, bronchial; bb, bronchiolar; AL, alveolar; SF_{BB}, scale factor for trachea; SF_{bb}, scale factor for bronchiolar; SF_{AL}, scale factor for alveolar; V, tidal or inhalation volume; Q, volumetric or inhalation flow rate; $t_{r,bb}$, residence time for bronchiolar; $t_{r,AL}$, residence time for alveolar; d_{ae}, aerodynamic particle diameter.
[$] Aerodynamic filtration efficiency for ET2 region was calculated as $\eta_{ae} = 1-1/(-aR^P+1)$

Table S2. Algebraic expressions for thermodynamic filtration efficiency in the ICRP 66 deposition model (ICRP, 1995).

Thermodynamic regional deposition efficiency ($\eta_{th} = 1-\exp(-aR^P)$)					
Phase	**Filter (j)**	**Region**	**a**	**R**	**P**
Inhalation	1	ET_2	9	$D \cdot (Q \cdot SF_{BB})^{-0.25}$	0.5
	2	BB	$22.02 \cdot SF_{BB}^{1.24} \cdot \Psi_{th}$	$D \cdot t_{r,BB}$	0.6391
	3	bb	$-76.8 + 167 \cdot SF_{bb}^{0.65}$	$D \cdot t_{r,bb}$	0.5676
	4	AL	$170 + 103 \cdot SF_{AL}^{2.13}$	$D \cdot t_{r,AL}$	0.6101
Exhalation	5	bb	$-76.8 + 167 \cdot SF_{bb}^{0.65}$	$D \cdot t_{r,bb}$	0.5676
	6	BB	$22.02 \times SF_{BB}^{1.24} \cdot \Psi_{th}$	$D \cdot t_{r,BB}$	0.6391
	7	ET_2	9	$D \cdot (Q \cdot SF_{BB})^{-0.25}$	0.5

where a and P are constants and R is a parameter, which is drug- and system-dependent. a, P and R were obtained from ICRP 66 deposition model (ICRP, 1995). ET2, extrathoracic (oral passage); BB, bronchial; bb, bronchiolar; AL, alveolar; SF_{BB}, scale factor for trachea; SF_{bb}, scale factor for bronchiolar; SF_{AL}, scale factor for alveolar; Q, volumetric or inhalation

flow rate; $t_{r,BB}$, residence time for bronchial; $t_{r,bb}$, residence time for bronchiolar; $t_{r,AL}$, residence time for alveolar; D, diffusion coefficient; d_{th}, thermodynamic particle diameter. $^{\#}\Psi_{th}$ is an empirical correction factor to allow for enhancement of thermodynamic deposition caused by nonlaminar bronchial airflow and calculated $\Psi_{th} = 1+100\ \exp[-[\log_{10}(100+10/(d_{th}^{0.9}))]^2]$

Table S3. Algebraic expressions for a volumetric fraction in the ICRP 66 deposition model (ICRP, 1995).

Phase	Filter (j)	Region	Volumetric fraction (ϕ_j)
Inhalation	1	ET_2	1
	2	BB	$1 - (V_{D,ET2}/V)$
	3	bb	$1 - ((V_{D,ET2} + V_{D,BB,p})/V)$
	4	AL	$1 - ((V_{D,ET2} + V_{D,BB,p} + V_{D,bb,p})/V)$
Exhalation	5	bb	$1 - ((V_{D,ET2} + V_{D,BB,p})/V)$
	6	BB	$1 - (V_{D,ET2}/V)$
	7	ET_2	1

FRC, functional residual capacity; V_D, dead space volume; ET2, extrathoracic (oral passage); BB, bronchial; bb, bronchiolar; AL, alveolar; V, tidal or inhalation volume. $V_{D,BB,p}$ and $V_{D,bb,p}$ were calculated as $V_{D,BB,p} = V_{D,BB} \times (1 + (V/FRC))$ and $V_{D,bb,p} = V_{D,bb} \times (1 + (V/FRC))$, respctively.

Table S4. Respiratory tissue-specific input parameters for the OI-PBPK model (ICRP, 1995; Patton and Byron, 2007).

	Extra-thoracic (ET2)	Bronchial (BB)	Bronchiolar (bb)	Alveolar (AL)
Surface area (SA, cm^2)	450	290	2400	1475000
ELF thickness (um)	15	11	6	0.07
Epithelial thickness (cm)	50	55	15	0.361
Subepithelial thickness (cm)	15	500	20	1.86
ELF volume (mL)	0.68	0.32	1.44	10.33
Epithelial volume (mL)	2.25	1.60	3.60	276
Subepithelial volume (mL)	0.68	14.50	4.80	274
Blood volume (mL)	17.73	11.43	94.57	556.5
Tissue volume (mL)	2.93	16.1	8.4	550
Density (g/mL)	1	1	1	1
Blood flow rate (L/h)	1.63	1.05	8.70	390.00
Respiratory transit time (h)	0.24	2.4	12	1200
Respiratory transit rate (1/h)	4.17	0.417	0.083	0.00083
Lymph flow (L/h)	0.002	0.0001	0.009	0.42
pH of ELF*	6.6	6.6	6.6	6.6
pH of epithelial*	6.69	6.69	6.69	6.69
pH of subepithelial$^{\#}$	7.35	7.35	7.35	7.35
pH of blood$^{\#}$	7.4	7.4	7.4	7.4

1. Volume of ELF, epithelial and subepithelial compartments of each region of the respiratory tract were calculated multiplying the SA of the compartment by the thickness of the compartment.

2. Volume of blood compartment of AL region was calculated by multiplying the total blood volume (5.3 L for adult male, ICRP Valentin) by the % total blood volume of pulmonary tissue (10.5% for adult male, ICRP Valentin).

3. Volume of blood compartment of BB and bb regions were calculated by multiplying the total blood volume (5.3 L for adult male, ICRP Valentin) by the % total blood volume of bronchial tissue (2% for adult male, ICRP Valentin) and $SA_{BB\ or\ bb}/SA_{BB+bb}$.

4. Blood flow of BB and bb regions were calculated by multiplying cardiac output (390 L/h for adult male, ICRP Valentin) by the % cardiac output of bronchial tissue (2.5% for adult male, ICRP Valentin) and $SA_{BB\ or\ bb}/SA_{BB+bb}$.

5. Blood flow or volume of ET2 region were calculated by multiplying blood flow or volume of BB region by the SA_{ET2}/SA_{BB} due to unavailability of data and SA of ET2 is comparable to that of BB region.

6. Lymph flow of each region was calculated by dividing plasma flow (multiplying blood flow of each reagion by 1- hematocrit (0.46)) by 500 (Shah et al., 2012).

*(Gaohua et al., 2015)

#(Burton, 2001)

Table S5. Summary of system-dependent parameters for the reference adult male (Valentin, 2002)*

	Organ Volume (L)	**Blood flow (% of CO)**	**Blood flow (L/h)**
Adipose	18.2	5	19.50
Bone	10.5	5	19.50
Brain	1.45	12	46.80
Gut**	1.21	15	58.50
Heart	0.33	4	15.60
Kidney	0.31	19	74.10
Liver	1.8	25.5	99.45
Hepatic artery		6.5	25.35
Muscle	29	17	68.25
Skin	3.3	5	19.50
Spleen	0.15	3	11.70
Pancreas	0.14	1	3.90
Lymph nodes	0.274$	1.7	6.63
Blood	5.3		

*Reference values for adult male: 35 years of age, 73 kg of body weight, 176 cm of height and 390 L/h of cardiac output (CO). ** Gut combines oesophagus, stomach, small and large intestine volumes and flows; gut contents were not included in the gut volume.

$(Shah et al., 2012)

Table S6. Summary of input parameters for the morphine OI-PBPK model.

Parameter	Value/method/model	Reference
Physicochemical and blood binding		
MW (g/mol)	285.34	(Emoto et al., 2017)
Log $P_{o:w}$	0.77	(Emoto et al., 2017)
pKa1, pKa2	9.63, 7.93	(Emoto et al., 2017)
Compound type	Ampholyte	
B/P	1.08	(Emoto et al., 2017)
fu	0.62	(Emoto et al., 2017)
Distribution		
Model	Full PBPK	(Emoto et al., 2017)
Method	Rodgers et al Method 2	(Emoto et al., 2017)
Organ/tissue Kp		(Emoto et al., 2017)
Adipose	1.079	
Bone	2.092	
Brain	1.517	
Gut	7.228	
Heart	7.737	
Kidney	4.187	
Liver	12.417	
Lung	1.970	
Muscle	6.597	
Skin	3.521	
Spleen	7.273	
Pancreas	4.771	
Kp scalar	1	
Elimination		
CL_R in L/h	8	(Emoto et al., 2017)
Organ/tissue	Liver	(Emoto et al., 2017)
Pathway: 6MG		
Enzyme	UGT2B7	
V_{max} (pmol/min/mg protein)	1917	
K_m (μM)	115.8	
fu_{mic}	1	
V_{max} (μmol/h)	6625.15	
Pathway: 3MG		

Enzyme	UGT2B7	
V_{max} (pmol/min/mg protein)	9250	
K_m (µM)	115.8	
fu_{mic}	1	
V_{max} (µmol/h)	31968	
Transport		
Organ/Tissue	Liver	(Emoto et al., 2017)
$CL_{PD,in\ vitro}$ (mL/min/10^6 cells)	0.003	
$CL_{PD,organ}$ (L/h)	32.1	
fu_{IC}	0.05	Eq. 35
fu_{IS}	1	Eq. 36
Organ/Tissue	Liver	
Transporter	SLC22A1 (OCT1)	
Location	Sinusoidal	
Function	Influx	
J_{max} (pmol/min/10^6 cells)	29	
K_m (µM)	3.4	
fu_{inc}	1	
RAF/REF	5.1	
J_{max} (µmol/h)	1584.4	Eq. 55
Liver: PSF		
HPGL (hepatocellularity /g liver or 10^6 cells/g liver)	99	(Barter et al., 2007)
Liver weight (g)	1800	Table S5
Liver: UGT2B7		
A_{UGT2B7} (pmol/mg microsomal protein)	75.2	(Ladumor et al. 2019)
A_{UGT2B7} (µmol/liver tissue)	4.3	Eq. 58
Liver: OCT1		
A_{OCT1} (pmol/mg membrane protein)	4.45	
A_{OCT1} (µmol/liver tissue)	0.30	Eq. 58
Liver: PSF		
MMPGL (mg microsomal protein/g liver)	32	(Barter et al., 2007)
MMePGL (mg membrane protein/g liver)	37	(Prasad et al., 2014)
Lung: UGT2B7		
A_{UGT2B7} (pmol/mg microsomal protein)[1]	0.15	

A_{UGT2B7} (µmol/lung tissue)	BB:9E-6 bb: 5E-6 AL: 3E-4	Eq. 58
Lung: OCT1		
A_{OCT1} (pmol/mg membrane protein)[2]	0.22	(Wang et al. 2015)
A_{OCT1} (µmol/lung tissue)	BB:1E-5 bb: 7E-6 AL: 5E-4	Eq. 58
Lung: PSF		
MMPGLu (mg microsomal protein/g lung)	3.8	(Pacifici et al., 1988)
MMePGLu (mg membrane protein/g lung)[3]	3.8	(Pacifici et al., 1988)

MW, molecular weight; Log $P_{o:w}$, n-octanol/water partition coefficient; pK_a, acid dissociation constant; B/P, blood/plasma ratio; fu, fraction of unbound drug in the plasma; HSA, human serum albumin; K_p, tissue to plasma partition coefficient; V_{max}, maximum enzymatic reaction rate; J_{max}, maximum transport rate; K_m, substrate affinity or Michaelis-Menten constant; fu_{mic}, fraction of unbound drug in the vitro microsomal incubation; fu_{inc}, fraction of unbound drug in the *vitro* incubation; fu_{IC}, fraction of unbound drug in the intracellular compartment; fu_{IS}, fraction of unbound drug in the interstitial compartment; $CL_{PD, in\ vitro}$, in vitro passive diffusion clearance; $CL_{PD,organ}$, in vivo whole organ passive diffusion clearance; CL_R, renal clearance; RAF/REF, relative activity factor/relative expression factor; PSF, physiological scaling factor (yield of the subcellular fraction from whole organ (in mg subcellular fraction protein/g organ)); A_{DMET} is the protein abundance of drug metabolizing enzymes and transporters (DMET); UGT, uridine 5'-diphospho-glucuronosyltransferase; OCT, organic cation transporter; MMPGL, mg microsomal protein per gram of human liver; MMePGL, mg total membrane protein per gram of human liver; MMPGLu, mg microsomal protein per gram of human lung; MMePGLu, mg total membrane protein per gram of human lung; HPGL, hepatocellularity per gram of human liver.
1. UGT2B7 protein abundance per subcellular fraction was calculated by multiplying the liver subcellular protein abundance by the ratio of lung (BB, bb, and AL) to liver tissue mRNA expression (Somers et al., 2007).
2. OCT1 protein abundance per subcellular fraction was calculated by multiplying the liver subcellular protein abundance by the ratio of lung (BB, bb, and AL) to liver tissue transporter plasma membrane expression (Ohtsuki et al., 2012; Sakamoto et al, 2013).
3. MMePGLu was assumed similar to the MMPGLu.

Table S7. Summary of input parameters for the nicotine OI-PBPK model.

Parameter	**Value/method/model**	**Reference**
Physicochemical and blood binding		
MW (g/mol)	162.2	(Kovar et al., 2020)
Log $P_{o:w}$	1.6	(Kovar et al., 2020)
pKa1, pKa2	8.1, 3.3	(Kovar et al., 2020)
Compound type	Diprotic base	
B/P	1.03	(Kovar et al., 2020)
fu	0.951	(Kovar et al., 2020)
Distribution		

Model	Full PBPK	(Kovar et al., 2020)
Method	Rodger et al.	(Kovar et al., 2020)
Organ/tissue Kp		(Kovar et al., 2020)
Adipose	0.74	
Bone	1.27	
Brain	1.89	
Gut	2.90	
Heart	2.24	
Kidney	4.15	
Liver	3.96	
Lung	3.25	
Muscle	3.05	
Skin	1.1*	
Spleen	2.86	
Pancreas	2.46	
Kp scalar	1	
Elimination		
Organ/tissue: Liver		(Kovar et al., 2020)
Enzyme	**CYP2A6**	
k_{cat} (1/min) (smokers)	10.5	
K_m (µM)	29.4	
fu_{mic}	1	
V_{max} (µmol/h)	979.8	
Enzyme	**CYP2B6**	
k_{cat} (1/min) (smokers)	16	
K_m (µM)	820	
fu_{mic}	1	
V_{max} (µmol/h)	884.7	Eq. 55
Unspecified hepatic CL (1/min)	0.3	
Unspecified hepatic CL (L/min)	32.4	
CL_R in L/h	3.58	
Liver: CYP2A6		
A_{CYP2A6} (pmol/mg microsomal protein)	27	
A_{CYP2A6} (µmol/liver tissue)	1.56	Eq. 58
Liver: CYP2B6		

A_{CYP2B6} (pmol/mg microsomal protein)	16	
A_{CYP2B6} (μmol/liver tissue)	0.92	Eq. 58
Liver: PSF		
MMPGL (mg microsomal protein/g liver)	32	(Barter et al., 2007)
Liver weight (g)	1800	Table S5
Lung: CYP2A6		
A_{CYP2A6} (pmol/mg microsomal protein)[1]	0.11	
A_{CYP2A6} (μmol/liver tissue)	BB:7E-6 bb: 4E-6 AL: 2E-4	Eq. 58
Lung: CYP2B6		
A_{CYP2B6} (pmol/mg microsomal protein)[1]	0.16	
A_{CYP2B6} (μmol/lung tissue)	BB:1E-5 bb: 5E-6 AL: 3E-4	Eq. 58
Lung: PSF		
MMPGLu (mg microsomal protein/g lung)	3.8	(Pacifici et al., 1988)

MW, molecular weight; Log $P_{o:w}$, n-octanol/water partition coefficient; pK_a, acid dissociation constant; B/P, blood/plasma ratio; fu, fraction of unbound drug in the plasma; HSA, human serum albumin; K_p, tissue to plasma partition coefficient; k_{cat}, catalytic activity; V_{max}, maximum enzymatic reaction rate; K_m, Michaelis-Menten constant; fu_{mic}, fraction of unbound drug in the *in vitro* microsomal incubation; CL_R, renal clearance; PSF, physiological scaling factor (yield of the subcellular fraction from whole organ (in mg subcellular fraction protein/g organ)); A_{DME} is the protein abundance of drug metabolizing enzymes (DME); CYP, cytochromes P450; MMPGL, mg microsomal protein per gram of human liver; MMPGLu, mg microsomal protein per gram of human lung.

*Huang and Isoherranen, 2020.

1. CYP2A6 and CYP2B6 protein abundance per subcellular fraction were calculated by multiplying the liver subcellular protein abundance by the ratio of lung (BB, bb, and AL) to liver tissue mRNA expression (Somers et al., 2007).

Table S8. Input and output for predicting the DE of morphine (administered via a nebulizer) in each region of the respiratory tract using the ICRP 66 deposition model.

Input for the ICRP 66 deposition model		
Parameters	**Values**	**References**
Drug parameters		
MMAD (μm)	2.95	(Schuster et al., 1997)
GSD (dimensionless)	0	
Type	Monodisperse	Default (ICRP, 1995)
ρ (g/mL)	3	

X (dimensionless)	1.5	Default (ICRP, 1995)	
η_I (dimensionless)	1	Model predicted	
f_{hyg} (dimensionless)	3	Assumed	
DF_{scalar} (dimensionless)	1	Default	
Breathing parameters			
Breathing route	Mouth		
Activity type	Sitting		
Q (mL/s)	1208.33	(Dershwitz et al., 2000)	
V (mL)	500	(Dershwitz et al., 2000)	
U (m/s)	1	(Klumpp and Bertelli, 2017)	
Systems parameters			
FRC (mL)	3301	Adult male (ICRP, 1995)	
$V_{D,ET}$ (mL)	50	Adult male (ICRP, 1995)	
$V_{D,BB}$ (mL)	49	Adult male (ICRP, 1995)	
$V_{D,bb}$ (mL)	47	Adult male (ICRP, 1995)	
$V_{D,total}$ (mL)	146	Adult male (ICRP, 1995)	
SF_{BB} (dimensionless)	1	Adult male (ICRP, 1995)	
SF_{bb} (dimensionless)	1	Adult male (ICRP, 1995)	
SF_{AL} (dimensionless)	1	Adult male (ICRP, 1995)	
Output of the ICRP 66 deposition model			
Region	**DE**	**DE with f_{hyg}**	***In vivo* DE**
ET2	19.2	33.0	NA
BB	16.0	19.5	NA
bb	7.1	8.1	NA
TB (BB+bb)	23.2	27.6	NA
AL	10.4	12.3	NA
Total	52.8	72.9	NA
Exhaled	47.2	27.1	NA
TB (central)/AL (peripheral)	2.22	2.24	NA

MMAD, mass median aerodynamic diameter; GSD, geometric standard deviation of aerodynamic diameter; Q, volumetric or inhalation flow rate; V, tidal or inhalation volume; DE, deposition efficiency (%); ET2, extrathoracic (oral passage); BB, bronchial; bb, bronchiolar; TB, tracheobronchial; AL, alveolar; f_{hyg}, hygroscopic growth factor; DF_{scalar}, empirical scaling factor to scale regional deposition fraction; ρ, drug density; χ, shape factor; η_I, inhalibility.

Table S9. Input and output for predicting the DE of nicotine (administered via cigarette smoking) in each region of the respiratory tract using the ICRP 66 deposition model.

Input for the ICRP 66 deposition model				
Parameters	**Values**	**References**		
Drug parameters				
MMAD (μm)	0.4	(Schroeter et al., 2001)		
GSD (dimensionless)	0			
Type	Monodisperse			
ρ (g/mL)	3	Default (ICRP, 1995)		
X (dimensionless)	1.5	Default (ICRP, 1995)		
η_I (dimensionless)	1	Model predicted		
f_{hyg} (dimensionless)	1.7	(Schroeter et al., 2001)		
DF_{scalar} (dimensionless)	1.5	Estimated to recover *in vivo* deposition		
Breathing parameters				
Breathing route	Mouth			
Activity type	Sitting			
Q (mL/s)	17.5	Calculated using puff volume (35 mL) and puff time (2 s) (Kane et al., 2010)		
V (mL)	500	(Kane et al., 2010)		
U (m/s)	1	(Klumpp and Bertelli, 2017)		
Systems parameters				
FRC (mL)	3301	Adult male (ICRP, 1995)		
$V_{D,ET}$ (mL)	50	Adult male (ICRP, 1995)		
$V_{D,BB}$ (mL)	49	Adult male (ICRP, 1995)		
$V_{D,bb}$ (mL)	47	Adult male (ICRP, 1995)		
$V_{D,total}$ (mL)	146	Adult male (ICRP, 1995)		
SF_{BB} (dimensionless)	1	Adult male (ICRP, 1995)		
SF_{bb} (dimensionless)	1	Adult male (ICRP, 1995)		
SF_{AL} (dimensionless)	1	Adult male (ICRP, 1995)		
Output of the ICRP 66 deposition model				
Region	**DE**	**DE with f_{hyg}**	**DE with f_{hyg} and DF_{scalar}**	***In vivo* DE**
ET2	1.0	0.7	1.1	
BB	2.0	1.3	2.0	
bb	31.3	41.1	61.7	
TB (BB + bb)	33.3	42.4	63.7	42-63*
AL	21.4	20.8	31.2	26-35*

Total	55.7	64	96.0	86-97[#]
Exhaled	44.3	36	4.0	
TB (central)/AL (peripheral)	1.55	2.04	2.04	

MMAD, mass median aerodynamic diameter; GSD, geometric standard deviation of aerodynamic diameter; Q, volumetric or inhalation flow rate; V_T, tidal or inhalation volume; ET2, extrathoracic (oral passage); BB, bronchial; bb, bronchiolar; TB, tracheobronchial; AL, alveolar; f_{hyg}, hygroscopic growth factor; DF_{scalar}, empirical scaling factor to scale regional deposition fraction; ρ, drug density; χ, shape factor; η_I, inhalibility; DE, deposition efficiency in percent.

*(Broday and Robinson, 2003), #(Hinds et al., 1983)

Table S10. Summary of input parameters for morphine and nicotine OI model.

Parameter	**Morphine**	**Nicotine**	**Equations**
$Kp_{int\text{-}pls}$	0.74	0.93	Eq. 38
$P_{app,\ calu\text{-}3}$ (cm/s)	4.54E-06	8.62E-06	Eq. 42
P_{scalar}	2.4	-	
Thickness factor			Eq. 41
ET2	1.10	1.10	
BB	1.00	1.00	
bb	3.67	3.67	
AL	152.35	152.35	
$P_{app,\ n}$ (cm/s)			Eq. 40
ET2	4.99E-06	9.48E-06	
BB	4.54E-06	8.62E-06	
bb	1.66E-05	3.16E-05	
AL	6.92E-04	1.31E-03	
P_{mem} or PS (L/h)			Eq. 39
ET2	1.94E-02	1.54E-02	
BB	1.14E-02	9.00E-03	
Bb	3.46E-01	2.73E-01	
AL	8.81E+03	6.97E+03	
Regions: ET2, BB, bb and AL			Eqs. 28-33
fui_F	0.04	0.97	
fui_E	0.06	0.96	
fui_S	0.21	0.15	
fui_B	0.23	0.17	
Regions: ET2, BB, bb and AL			Eqs. 34-37

fu_F fu_E fu_S fu_B	1 0.31 0.84 0.57	1 0.29 1 0.92	
Regions: ET2, BB, bb and AL CLinf,F-E (L/h) CLeff,E-F (L/h) CLinf,S-E (L/h) CLeff,E-S (L/h)	 NA NA NA NA	 NA NA NA NA	
Regions: ET2, BB, bb and AL CL_{int} (L/h)	 NA	 NA	
Regions: ET2, BB, bb and AL k_{deg} (1/h)	 NA	 NA	
Regions: ET2, BB, bb and AL k_{on} (L/mg/h) k_{off} (1/h)	 NA NA	 NA NA	

Table S11. Comparison of simulated and observed PK parameters of morphine after IV infusion (IV Inf) or oral inhalation (OI; nebulizer)

Study ID	Dosing regimen	PK parameters	Simulated	Observed	Ratio
Dershwitz et al_2000	IV Inf Dose: 8.8 mg Duration: 0.16 h	C_{max}	258.0	261.1	0.99
		AUC_{last}	66.8	66.05	0.97
Dershwitz et al_2000 (without f_{hyg})	OI (dose: 2.2 mg, no. of dose: 8; interval: 1 min)	C_{max}	76.5	120.3	0.64
		AUC_{last}	37.8	71.8	0.53
Dershwitz et al_2000 (with f_{hyg})	OI (dose: 2.2 mg, no. of dose: 8; interval: 1 min)	C_{max}	91.8	120.3	0.76
		AUC_{last}	46.5	71.8	0.65
Dershwitz et al_2000 (with f_{hyg} and P_{scalar})	OI (dose: 2.2 mg, no. of dose: 8; interval: 1 min)	C_{max}	139.4	120.3	1.16
		AUC_{last}	65.3	71.8	0.91

f_{hyg}, hygroscopic growth factor; P_{scalar}, permeability scalar, used to scale the epithelial apical permeability; C_{max}, maximum plasma concentration; AUC_{last}, area under the plasma concentration-time curve from 0 to the last measured time point.

Table S12. Comparison of the simulated and observed PK parameters of nicotine after IV infusion.

Study ID	Dosing regimen	PK parameters	Simulated	Observed	Ratio
Gourlay and Benowitz_1997	IV Inf (4.38 mg)	C_{max}	28.1	28.65	0.98
		$AUC_{0\text{-last}}$	17.5	19.44	0.90
Benowitz and Jacob_1994	IV Inf (60 µg/kg)	C_{max}	27.1	24.06	1.13
		$AUC_{0\text{-last}}$	50.6	51.24	0.99

Table S13. Comparison of the simulated and observed PK parameters of nicotine after oral inhalation (cigarette smoking) when f_{hyg} and DF_{scalar} were incorporated.

Study ID	Dosing regimen*	PK parameters	Simulated	Observed	Ratio
Gourlay and Benowitz 1997	OI (Dose: 0.22 mg; No. of puff: 10; Puff interval: 1 min)	C_{max}	19.9	19.18	1.04
		$AUC_{0\text{-last}}$	11.1	10.36	1.07
Fearson et al. 2017	OI (Dose: 0.13 mg; No. of puff: 10; Puff interval: 0.0083 h)	C_{max}	12.2	11.95	1.02
		$AUC_{0\text{-last}}$	2.4	2.12	1.14
Fearson et al. 2017	OI (Dose: 0.07 mg; No. of puff: 10; Puff interval: 0.0083 h)	C_{max}	6.6	6.29	1.04
		$AUC_{0\text{-last}}$	3.6	3.59	1.01
St. Helen et al. 2019	OI (Dose: 0.24 mg; No. of puff: 10; Puff interval: 0.0083 h)	C_{max}	22.5	20.53	1.09
		$AUC_{0\text{-last}}$	25.7	23.05	1.11

*doses adopted from Kovar et al., 2020.

Supplemental Figures

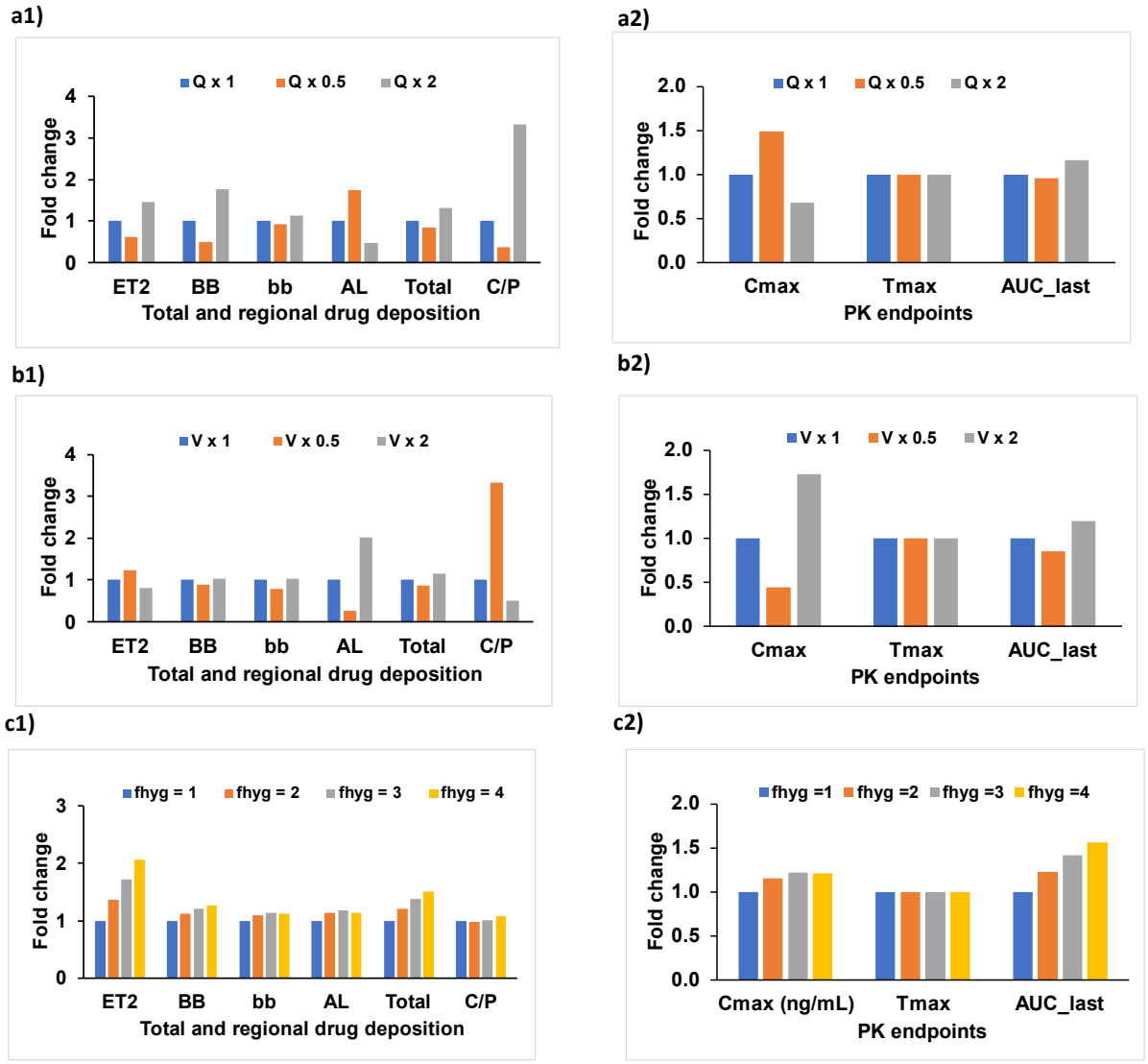

Fig. S1. Sensitivity analyses to demonstrate the impact of change in inhalation flow (a1 and a2), inhalation volume (V; b1 and b2), and hygroscopic growth factor (f_{hyg}; c1 and c2)) on total and regional respiratory tract deposition, as well as pharmacokinetic (PK) endpoints of drug X. ET2, extrathoracic (oral passage); BB, bronchial; bb, bronchiolar; AL, alveolar; C, central region (BB+bb); P, peripheral region (AL).

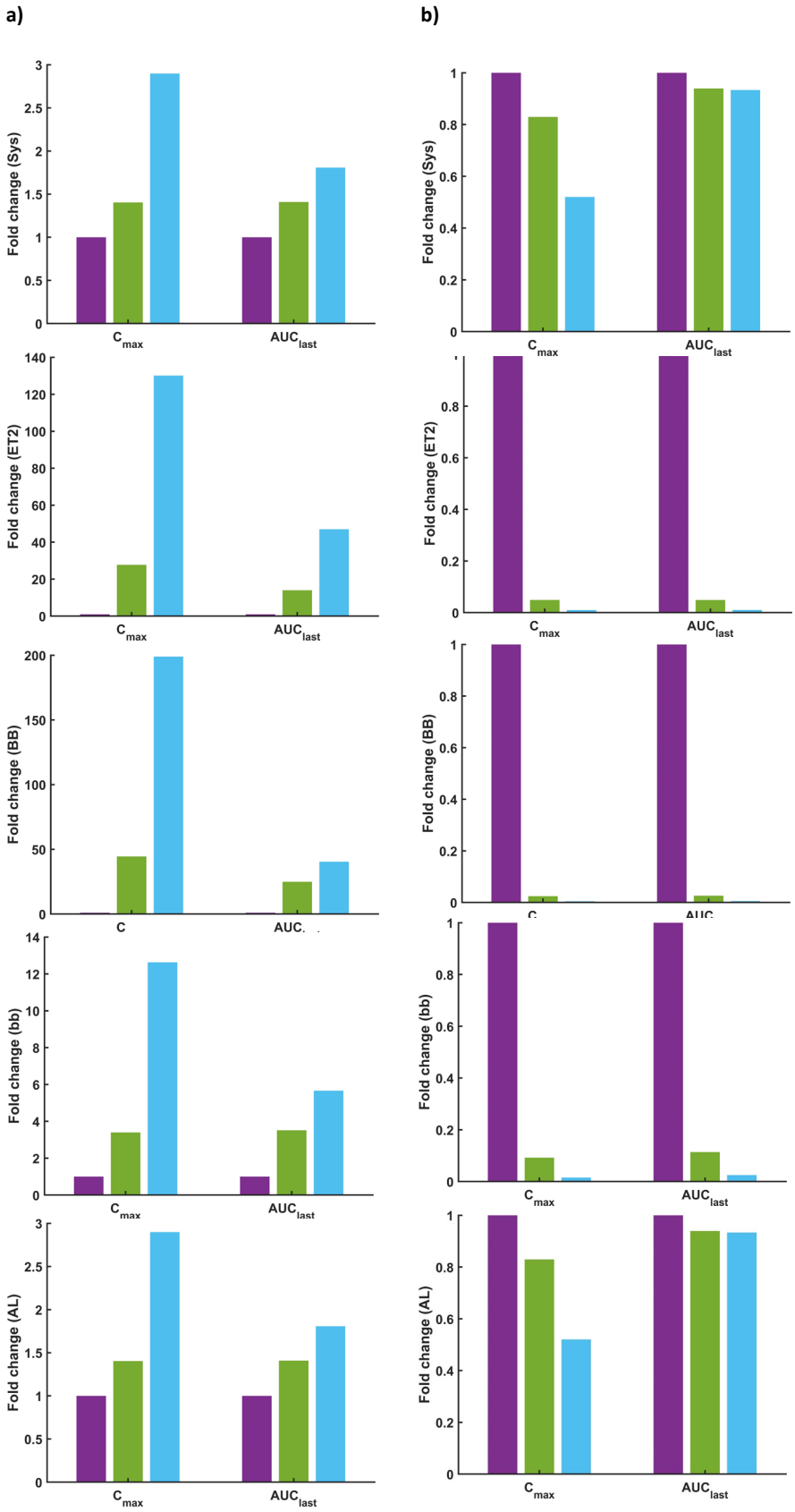

Fig. S2. Sensitivity analyses to demonstrate the impact of epithelial membrane transport on systemic and local epithelial concentrations of drug Y in various regions of the respiratory

tract (ET2, BB, bb and AL) in the presence of a) apical influx transport (clearance: 0 L/h, purple color; 0.0001 L/h, green color; 0.0005 L/h, sky blue color); or b) apical efflux transport (clearance: 0 L/h, purple color; 50 L/h, green color; 250 L/h, sky blue color). In all the cases, low apparent passive permeability (4.54e-8 cm/s) between ELF and epithelial was unchanged. Increased influx or efflux apical epithelial membrane transport results in either increased (influx) or reduced (efflux) drug Y epithelial concentrations in all the regions of the respiratory tract except for the AL region (because of the lower drug's AL deposition in the ELF compartment and large AL surface area, resulting in high passive drug permeability).

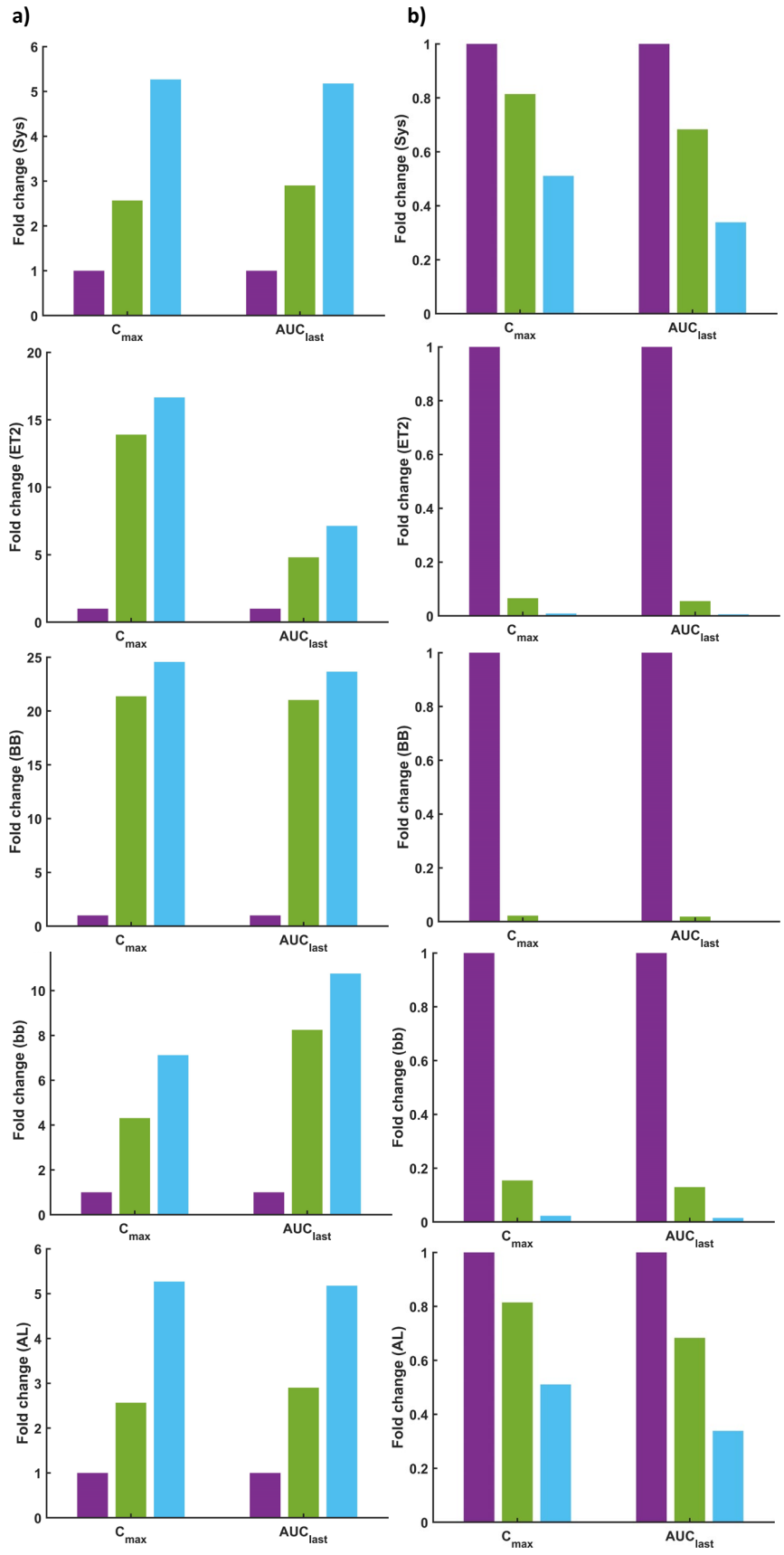

Fig. S3. Sensitivity analyses to demonstrate the impact of apical subepithelial membrane (or basal epithelial membrane) transport on systemic and local subepithelial concentrations of

drug Y in various respiratory tract compartments (ET2, BB, bb and AL) in the presence of a) influx transport (clearance: 0 L/h, purple color; 50 L/h, green color; 250 L/h, sky blue color); or b) efflux transport (clearance: 0 L/h, purple color; 10 L/h, green color; 50 L/h, sky blue color). In all the cases, low apparent passive permeability (4.54e-8 cm/s) between ELF and epithelial as well as epithelial and subepithelial was unchanged. Increased influx or efflux subepithelial membrane transporter activity results in increased (influx) or reduced (efflux) drug Y epithelial concentrations in all the regions of the respiratory tract.

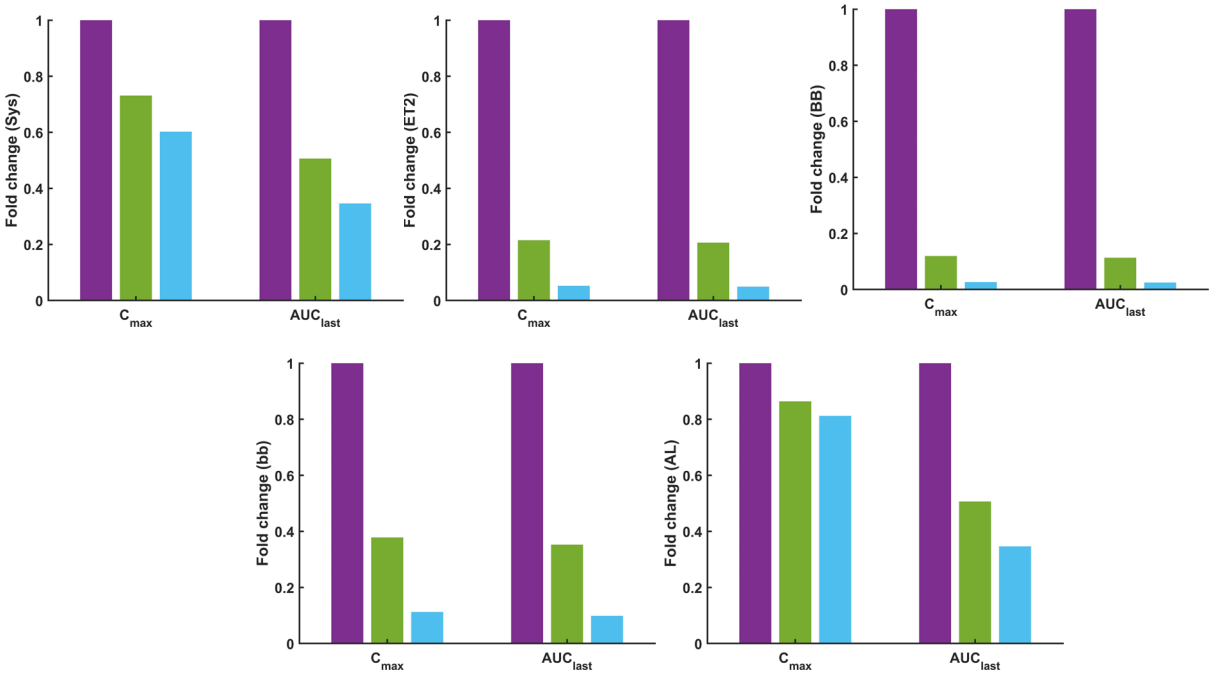

Fig. S4. Sensitivity analyses to demonstrate the impact of epithelial metabolism on systemic and local epithelial concentrations of drug Y in various lung compartments (ET2, BB, bb and AL) in the presence of metabolism (clearance: 0 L/h, purple color; 10 L/h, green color; 50 L/h, sky blue color). Increased drug metabolic activity in the epithelial region, decreased systemic and regional exposure of drug Y.

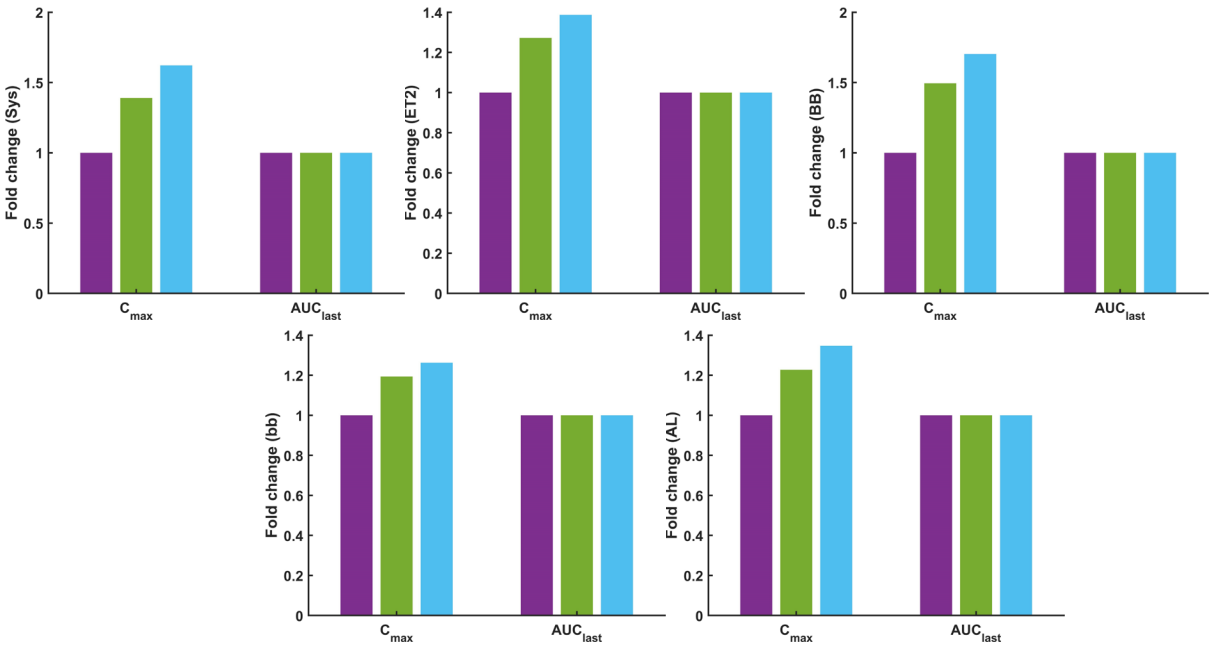

Fig. S5. Sensitivity analyses to demonstrate the impact of tissue retention on systemic and local epithelial concentrations of drug Y in various respiratory tract compartments (ET2, BB, bb and AL) in the presence of tissue retention (dissociation rate constant: 10 1/h, purple color; 50 1/h, green color; 250 1/h, sky blue color; in all these cases, the association rate constant and fatty acid concentrations were fixed to 50 L/mg/h and 10.0 mg/L). Increased dissociation rate constant in the epithelial region, increased systemic and regional C_{max} but did not change exposure to drug Y (AUC_{last}).

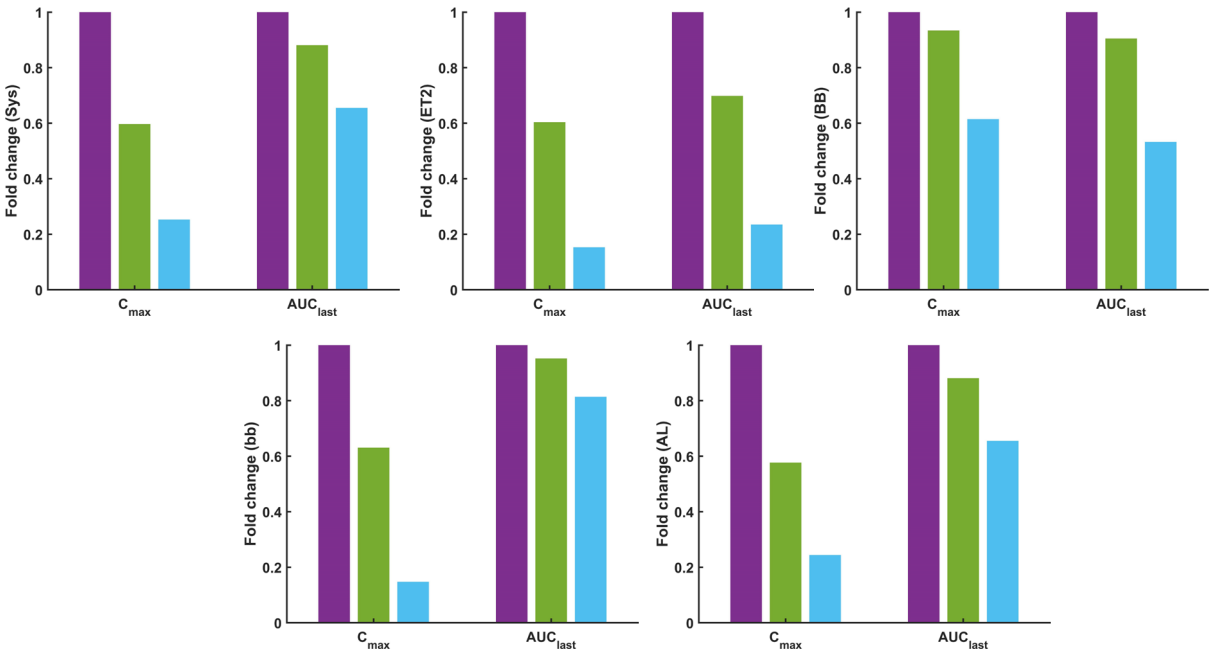

Fig. S6. Sensitivity analyses to demonstrate the impact of dissolution rate (z-factor) on systemic and local epithelial concentrations of drug X in various respiratory tract compartments (ET2, BB, bb and AL) in the presence of dissolution rate (z-factor 0.01 L/mg/h, purple color; 0.001 L/mg/h, green color; 0.0001 L/mg/h, sky blue color). Decreased in the dissolution rate of drug X resulted in a decrease in both local and systemic C_{max} as well as AUC_{last} due to slow drug release in the airway fluid.

References:

Barter ZE, Chowdry JE, Harlow JR, Snawder JE, Lipscomb JC, Rostami-Hodjegan A (2008) Covariation of human microsomal protein per gram of liver with age: absence of influence of operator and sample storage may justify interlaboratory data pooling. *Drug Metabolism and Disposition* **36:**2405-9.

Brillault J, De Castro WV, and Couet W (2010) Relative contributions of active mediated transport and passive diffusion of fluoroquinolones with various lipophilicities in a Calu-3 lung epithelial cell model. *Antimicrobial Agents and Chemotherapy* **54:**543-545.

Broday DM and Robinson R (2003) Application of cloud dynamics to dosimetry of cigarette smoke particles in the lungs. *Aerosol Science & Technology* **37:**510-527.

Burton RF (2001) Differences in pH between interstitial fluid and arterial blood in water-breathing and air-breathing vertebrates. *Physiological and Biochemical Zoology* **74:**607-615.

Chen B, Namenyi J, Yeh H, Mauderly J, and Cuddihy R (1990) Physical characterization of cigarette smoke aerosol generated from a Walton smoke machine. *Aerosol Science and Technology* **12:**364-375.

Dershwitz M, Walsh JL, Morishige RJ, Connors PM, Rubsamen RM, Shafer SL, and Rosow CE (2000) Pharmacokinetics and pharmacodynamics of inhaled versus intravenous morphine in healthy volunteers. *The Journal of the American Society of Anesthesiologists* **93:**619-628.

Emoto C, Fukuda T, Johnson T, Neuhoff S, Sadhasivam S, and Vinks A (2017) Characterization of contributing factors to variability in morphine clearance through PBPK modeling implemented with OCT1 transporter. *CPT: pharmacometrics & Systems Pharmacology* **6:**110-119.

Gaohua L, Wedagedera J, Small B, Almond L, Romero K, Hermann D, Hanna D, Jamei M, and Gardner I (2015) Development of a multicompartment permeability-limited lung pbpk model and its application in predicting pulmonary pharmacokinetics of antituberculosis drugs. *CPT: Pharmacometrics & Systems Pharmacology* **4:**605-613.

Hinds W, First M, Huber G, and Shea J (1983) A method for measuring respiratory deposition of cigarette smoke during smoking. *American Industrial Hygiene Association Journal* **44:**113-118.

Hintz RJ and Johnson KC (1989) The effect of particle size distribution on dissolution rate and oral absorption. *International Journal of Pharmaceutics* **51:**9-17.

ICRP (1995) ICRP publication 66: human respiratory tract model for radiological protection. Elsevier Health Sciences.

Kane DB, Asgharian B, Price OT, Rostami A, and Oldham MJ (2010) Effect of smoking parameters on the particle size distribution and predicted airway deposition of mainstream cigarette smoke. *Inhalation Toxicology* **22:**199-209.

Klumpp J and Bertelli L (2017) KDEP: a resource for calculating particle deposition in the respiratory tract. *Health Physics* **113:**110-121.

Kovar L, Selzer D, Britz H, Benowitz N, St. Helen G, Kohl Y, Bals R, and Lehr T (2020) Comprehensive parent-metabolite PBPK/PD modeling insights into nicotine replacement therapy strategies. *Clinical Pharmacokinetics* **59:**1119-1134.

Ladumor MK, Thakur A, Sharma S, Rachapally A, Mishra S, Bobe P, Rao VK, Pammi P, Kangne H, Levi D, Balhara A, Ghandikota S, Joshi A, Nautiyal V, Prasad B, and Singh S (2019) A repository of protein abundance data of drug metabolizing enzymes and transporters for applications in physiologically based pharmacokinetic (PBPK) modelling and simulation. *Scientific Reports* 9:9709.

Ohtsuki S, Schaefer O, Kawakami H, Inoue T, Liehner S, Saito A, Ishiguro N, Kishimoto W, Ludwig-Schwellinger E, Ebner T, Terasaki T (2012) Simultaneous absolute protein quantification of transporters, cytochromes P450, and UDP-glucuronosyltransferases as a novel approach for the characterization of individual human liver: comparison with mRNA levels and activities. *Drug metabolism and Disposition* **40:**83-92.

Pacifici GM, Franchi M, Bencini C, Repetti F, Di Lascio N, Muraro GB (1988) Tissue distribution of drug-metabolizing enzymes in humans. *Xenobiotica* **18:**849-56.

Patton JS and Byron PR (2007) Inhaling medicines: delivering drugs to the body through the lungs. *Nature Reviews Drug Discovery* **6:**67-74.

Po HN and Senozan N (2001) The Henderson-Hasselbalch equation: its history and limitations. *Journal of Chemical Education* **78:**1499.

Prasad B, Evers R, Gupta A, Hop CE, Salphati L, Shukla S, Ambudkar SV, Unadkat JD (2014) Interindividual variability in hepatic organic anion-transporting polypeptides and P-glycoprotein (ABCB1) protein expression: quantification by liquid chromatography tandem mass spectroscopy and influence of genotype, age, and sex. *Drug Metabolism and Disposition* **42:**78-88.

Sakamoto A, Matsumaru T, Yamamura N, Uchida Y, Tachikawa M, Ohtsuki S, and Terasaki T (2013) Quantitative expression of human drug transporter proteins in lung tissues: analysis of regional, gender, and interindividual differences by liquid chromatography-tandem mass spectrometry. *Journal of Pharmaceutical Sciences* 102:3395-3406.

Schmitt W (2008). General approach for the calculation of tissue to plasma partition coefficients. T*oxicology In Vitro* **22:**457-67.

Schroeter JD, Musante CJ, Hwang D, Burton R, Guilmette R, and Martonen TB (2001) Hygroscopic growth and deposition of inhaled secondary cigarette smoke in human nasal pathways. *Aerosol Science & Technology* **34:**137-143.

Schuster J, Rubsamen R, Lloyd P, and Lloyd J (1997) The AERx™ aerosol delivery system. *Pharmaceutical Research* **14:**354-357.

Shah DK, Betts AM (2012) Towards a platform PBPK model to characterize the plasma and tissue disposition of monoclonal antibodies in preclinical species and human. *Journal of Pharmacokinetics and Pharmacodynamics* **39:**67-86.

Somers GI, Lindsay N, Lowdon BM, Jones AE, Freathy C, Ho S, Woodrooffe AJ, Bayliss MK, Manchee GR (2007) A comparison of the expression and metabolizing activities of phase I and II enzymes in freshly isolated human lung parenchymal cells and cryopreserved human hepatocytes. Drug metabolism and disposition. **35**:1797-805.

Valentin J (2002) Basic anatomical and physiological data for use in radiological protection: reference values: ICRP Publication 89. *Annals of the ICRP* **32:**1-277.

Wang L, Prasad B, Salphati L, Chu X, Gupta A, Hop CE, Evers R, Unadkat JD (2015) Interspecies variability in expression of hepatobiliary transporters across human, dog, monkey, and rat as determined by quantitative proteomics. *Drug Metabolism and Disposition* **43:**367-74.